Integrated Millimeter-Wave and Terahertz Analyzers for Biomedical Applications

Dietmar Kissinger [ID], *Senior Member, IEEE*, Mehmet Kaynak, *Member, IEEE*, and Andreas Mai [ID], *Member, IEEE*

(Invited Paper)

Abstract—This invited paper reviews the progress of silicon-based integrated analyzers for biomedical applications over the last two decades. Focus is set on various integrated circuit realizations in the millimeter-wave range from 30 GHz and at the terahertz frequencies of above 300 GHz. This article discusses high-frequency architectures and concrete implementations of both narrowband as well as broadband integrated readout circuits, including their use in miniaturized sensor solutions. A variety of circuits ranging from low-power sensing oscillators to highly integrated broadband vector network analyzers (VNAs), and example realizations of millimeter-wave cardiovascular sensors and implants to THz microfluidic labs-on-chip and exhaled human breath analyzers are recapitulated. This article closes with an outlook on emerging fields of research for future advancement of such biomedical sensors toward reliable and specific systems.

Index Terms—BiCMOS integrated circuits, biomedical electronics, microfluidics, millimeter-wave circuits, sensor systems, submillimeter-wave circuits, transceivers.

I. INTRODUCTION

BIOMEDICAL technologies continue to experience high interest and fast development. The ever-increasing need for new tools of analysis, rapid and reliable diagnosis, and patient-specific health assessment is fueled by the challenges of aging western populations and increasing cost of healthcare systems. Both established and novel sensor technologies are an important part in this task, and the foundation to prevent and treat diseases, restore health, and extend the lifetime of a population. Among the broad spectrum of biomedical sensing principles, high-frequency electromagnetic electronics in the microwave and millimeter-wave range [1] can provide an important contribution and new modalities. Their technological maturity due to the unprecedented success of commercial

communication applications allows for the proliferation of solutions for miniaturized complex sensors and microsystems using reliable high-level integration and sensing schemes in low-cost mass market silicon technologies.

Radiation in the microwave to terahertz range is non-ionizing and has traditionally been used for radar monitoring [2] and material imaging [3]. Recently, however, advanced biomedical sensor systems for lab-on-chip and point-of-care diagnosis, smart implants, and mobile devices with the goal of fast and reliable diagnosis of the patient's conditions have been proposed. Within this frequency range, materials can be probed at the cellular and molecular levels. Therefore, it is possible to determine gaseous, fluid, and tissue compositions via their dielectric properties. Depending on their frequency, these electromagnetic waves can penetrate biocompatible coatings and human tissue to a certain extent, allowing for localized noninvasive measurements. In [4], a microfluidics-based sensor solution for enhanced cancer cell detection through the use of wideband microwave spectroscopy of single biological cells has been proposed [5]–[7]. In addition, various research on the noninvasive sensing of glucose levels has been performed [8]–[12]. Furthermore, different promising tissue diagnostics [13], including hydration monitoring [14] and cancer identification [15], exist. Finally, proteins and DNA [16] can be probed in the THz range, and recent publications have even proposed the detection of stress via THz emission [17].

For all of the aforementioned applications, affordable and easy-to-use miniaturized sensor solutions are highly desirable to trigger a widespread use [18]. In this regard, state-of-the-art silicon technologies provide both the necessary high-frequency performance with maximum frequencies of oscillation above 700 GHz [19] as well as the complex integration capability and reliability at low cost [20]. Also, high-frequency integrated analysis circuits have already been investigated in the context of built-in test circuitry for complex radar and communication frontends [21]–[23]. Consequently, dedicated realizations of highly integrated systems for biomedical applications in the microwave spectrum have emerged in the last decade [24].

This article focuses on the advances made in the realization of miniaturized biomedical analyzer electronics in the millimeter-wave and terahertz domain. These can be combined with various broadband or resonant passive sensing elements. Due to their high-frequency capability and proven

Fig. 1.   Block diagram of (a) transmission-based analyzer and (b) analyzer based on the readout of a stimulus manipulated by a sensor element.
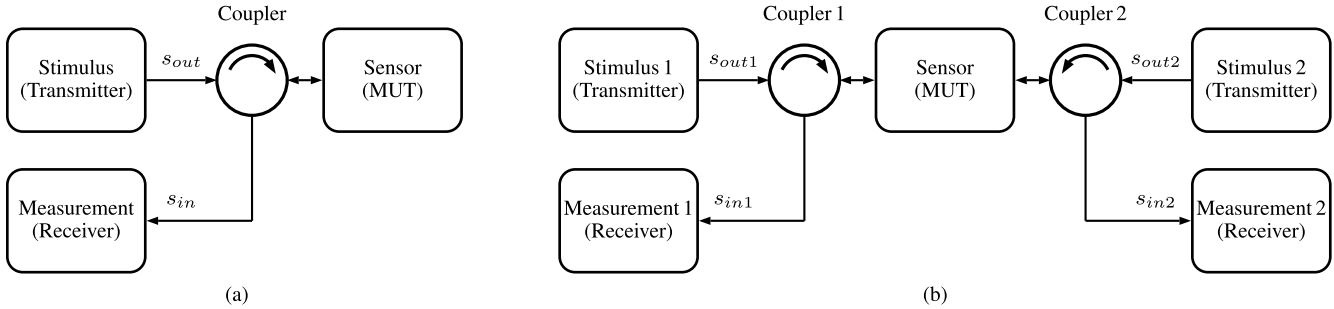
Fig. 2.   Block diagram of a general (a) reflectometer architecture with directional element and (b) two-port network analyzer comprised of two reflectometers.

success in radar and communication [25], SiGe BiCMOS technologies are a natural choice for such complex circuits [26]. After an overview on different architectures, highly integrated microsystems for microfluidic labs-on-chip, point-of-care spectroscopy systems, as well as invasives are presented. Finally, integrated multimodal sensor platforms with functionalization possibilities and future directions are discussed.

II. ANALYZER PRINCIPLES

A. Fundamentals

High-frequency biosensors are generally comprised of three parts: the sensor element, a stimulus for excitation of the former, and a readout circuit to determine the change of the stimulus after it has been affected by the varying sensor characteristic. The sensor is either an electromagnetic waveguide with field interaction to an external medium-under-test (MUT) or a radiating structure (antenna) for free-space media. Typical guided-wave sensor types in use are planar resonators or broadband transmission lines, depending on the need for high sensitivity or a broadband sensing range. The measurement circuit is used to quantitatively determine the changes of the stimulus wave due to the sensor element as a function of the changes in the MUT. These characteristics are typically amplitude (or power) and phase of the signal.

Fig. 1(a) shows a straightforward implementation of such a concept. It contains a circuit for stimulus generation and transmission, followed by a two-port sensor and a subsequent measurement channel, which is essentially a receiver (RX). This concept allows monitoring any change in the transmission behavior of a two-port sensor, such as a ring resonator [27]–[29] or a half-wavelength microstrip line resonator [30] due to the MUT. In a more advanced concept, the sensor can be included in the stimulus generator itself, for example, as the resonator in an oscillator tank, according to Fig. 1(b). This allows for power-efficient solutions, but introduces interdependencies of amplitude and phase change of the output signal.

If the sensor is a one-port device, such as a ring resonator in reflection mode [31], then a so-called reflectometer concept according to Fig. 2(a) can be used. Here, the introduction of a directional element, e.g., a circulator, hybrid, or directional coupler, allows for the separation of the incident stimulus and the reflected wave from the sensor. The reflectometer is the basic element of network analyzers and can be used to construct arbitrary-port systems. As an example, Fig. 2(b) shows a two-port network analyzer comprised of two reflectometers. The system can determine both reflection and transmission characteristics of the sensor. Most importantly it can account for the reduced transmission due to mismatches at the two ports and enables a more precise analysis.

In the high-frequency domain, the determination of voltages and currents is difficult due to very high or low impedance ports not being available. This has led to the concept of device characterization by means of scattering (S) parameters. The goal of this network analysis is the determination of the scattering matrix of a linear N-port network. For such a network, the relationship between all waves a_i traveling into and all waves b_i traveling out of an N-port can be written as a system of linear equations and given in a matrix form as $\mathbf{b} = \mathbf{Sa}$, where $\mathbf{S}$ represents the complex scattering matrix

$$\mathbf{S} = \begin{bmatrix} S_{11} & S_{21} \\ S_{12} & S_{22} \end{bmatrix} \quad \text{with}$$

$$S_{ij} = \left. \frac{b_i}{a_j} \right|_{a_k=0; k \neq j}. \tag{1}$$

The S-matrix consists of N^2 complex scattering coefficients S_{ij}. In this context, S_{ii} is commonly referred to as a reflection coefficient at port i, while S_{ij} is a transmission coefficient from port j to port i. All coefficients need to be determined by measuring the ratio of the wave b_i to the incident wave a_j, while the incident waves a_k of all other ports are required to be zero. This also implies that all other ports need to be terminated with matched loads to avoid any reflections [32].
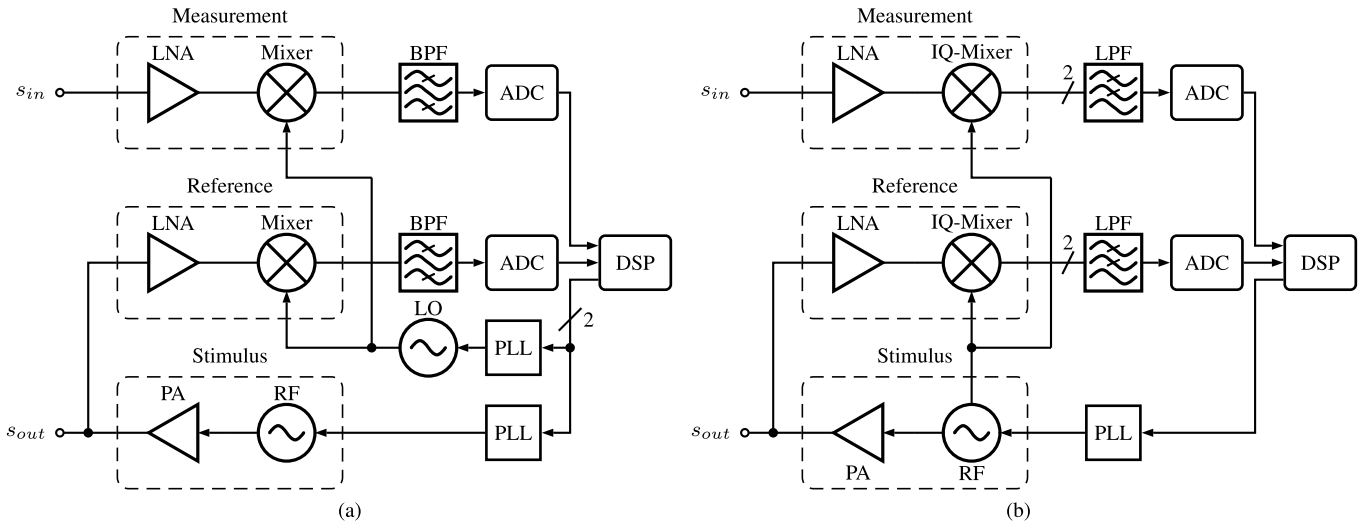
Fig. 3. Block diagrams of a mixer-based (a) heterodyne and (b) homodyne (direct conversion) reflectometer, excluding directional element/coupler [32].

The physical distance between analyzer and sensing element introduces additional attenuation and phase shifts. This does not necessarily pose a problem for the sensor system, but it is often desirable to perform a calibration to move the measurement reference plane to a desired interface to exclude parasitic effects and apply physical property extraction. Various methods with different complexity exist for a network analyzer calibration [33]. If the sensor element is located off-chip, it is possible to create a reference plane outside the analyzer by means of a set of on-wafer [34] or waveguide [35] calibration standards. More advanced methods employ electronically tunable on-wafer standards [36] or calibration by different reference MUTs [37] at the sensor.

B. Architectures

The concept of S-parameters can directly be mapped to a hardware architecture known as a vector network analyzer (VNA) [39]. The VNA not only features the aforementioned measurement channels of Fig. 2, but additionally includes reference channels for the identification of the incident-wave characteristics. Furthermore, the RF signals need to be down-converted in frequency. Although it is possible to do so by means of a noncoherent (power) detection scheme known as a scalar network analyzer [40]–[43], the simultaneous (complex) determination of the phase via coherent detection using a linear mixer scheme after Fig. 3 provides many advantages [44].

In complete analogy to modern radar or communication transceivers, the reflectometer can either feature a direct conversion or a heterodyne architecture [32]. Fig. 3(a) shows the block diagram of a heterodyne implementation of a reflectometer where the directional element has been omitted for simplicity. The concept requires two signal generators for the RF stimulus and local oscillator (LO) signal, which run at a fixed frequency offset to each other by means of a dual-loop phase-locked loop (PLL). This results in a downconversion of the complex RF signal to this IF offset frequency at the measurement and reference channels. Amplitude and phase of these channels are subsequently determined in the digital
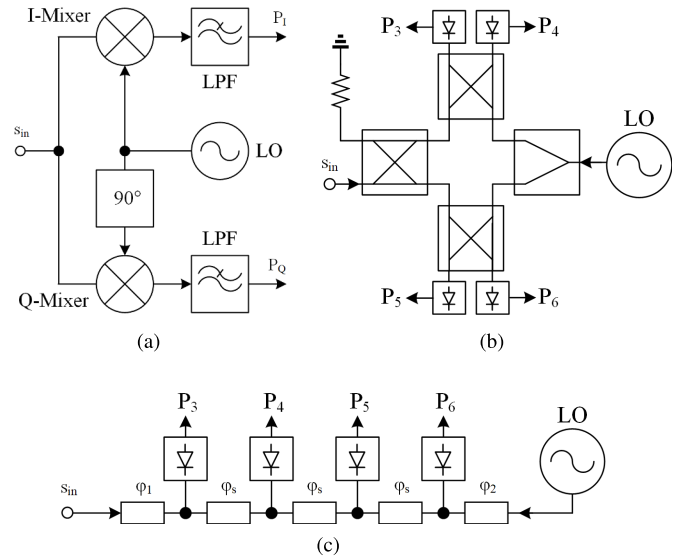
Fig. 4. Different implementations of a homodyne measurement or reference channel. (a) IQ mixer. (b) Six port. (c) Sampled line approach [38].

domain. In principle, an image-reject mixer is required, but the absence of signals in the image band in linear networks allows the use of single broadband (double sideband) mixers.

In contrast to the above, a homodyne or direct-conversion reflectometer architecture is shown in Fig. 3(b). Here, only a single signal source is used both as the RF stimulus as well as the LO signal for the mixers in the measurement and reference paths. To maintain the complex nature of the signal, an in-phase and quadrature (IQ) mixer is used to convert to the complex baseband. While the previous heterodyne concept requires an elaborate offset synchronization of the RF and LO signal, the homodyne approach suffers from dc offsets, limited bandwidth of the IQ phase shifters, and the necessity of twice as many analog-to-digital converters (ADCs).

Fig. 4(a) shows the IQ-mixer architecture in more detail. The 90° phase shifter is often split into two ±45° paths. While this concept has been used successfully in the past
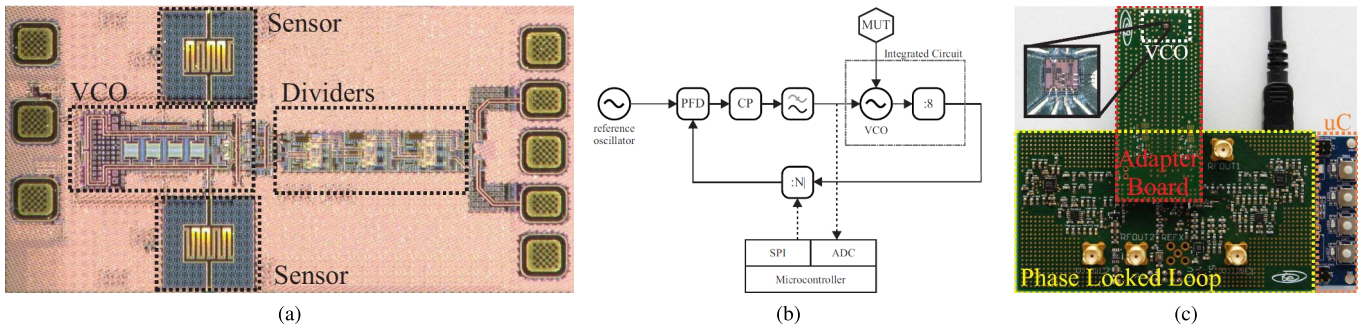
Fig. 5. (a) Chip photograph of a 20-GHz sensing oscillator and (b) related PLL-based readout architecture. (c) Permittivity sensor system demonstrator [55].
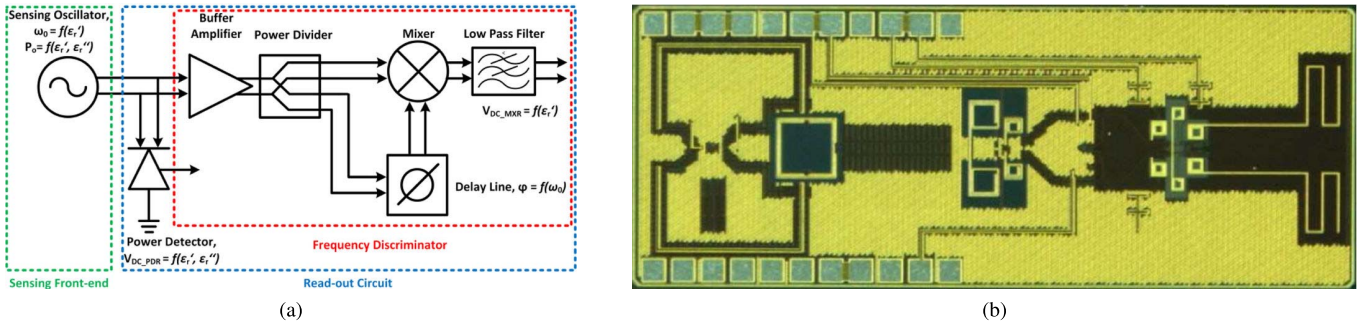
Fig. 6. (a) Block diagram and (b) chip photograph of a 30-GHz sensing oscillator with complex (power and frequency) readout circuit [56].

for transmission setups [45], reflectometers [46], as well as two-port VNAs [47], another popular approach is based on the so-called six port [48]. Depicted in Fig. 4(b), this architecture is based on the superposition of the LO and RF signal at four different phase differences to each other and subsequent additive mixing at individual detectors. Both six-port reflectometers [49]–[51] and a two-port VNA [52] have been demonstrated. Finally, the block diagram of a sampled-line RX is shown in Fig. 4(c). It can be considered as a simple six port [53] where the wave interference pattern along a transmission line is sampled by three to four detectors. This enables the computation of the amplitude and phase from simple scalar measurements [54].

III. READOUT CIRCUITS

A. Sensing Oscillators

The use of oscillators as sensing elements after the concept of Fig. 1(b) is a very popular approach. It combines the tasks of test signal (stimulus) generation and the interaction with a passive sensor structure. The latter is typically realized as part of the resonator (tank) within the oscillator, which defines the frequency of oscillation. Fig. 5(a) shows an example of a 20-GHz sensing oscillator, where the tank capacitance has been realized in the top gold metal layer, acting as a variable capacitor. Interaction of the passive tank sensor with an external MUT alters the attenuation and capacitance of the element, which leads to both a change of the oscillator output power and, most importantly, the frequency [57]. The intrinsic sensitivity of such an oscillator sensor is limited by its phase noise [58], and it is often used in conjunction with a reference oscillator in close proximity that can reduce process and temperature variation, drift dependencies, and other correlated

effects [59]. Finally, when moving into the millimeter-wave frequency range, many geometrically small oscillators can be used to enable spatial sensing over a certain area, as shown in [60] by means of 60- and 120-GHz 2-D arrays.

Various methods for the readout of an integrated oscillator-based sensor exist. After division to low frequencies, a frequency detector or counter can be used, requiring an additional reference signal. Furthermore, a properly designed filter with preceding buffer can be used to convert the frequency information into an amplitude, which can then be detected. In the microwave frequency range, however, a practical concept is the embedding of the oscillator in a PLL [61], [62]. An example of such a PLL-based readout is shown in Fig. 5(b) and (c) [55]. As a minimum, the general concept requires a voltage-controlled oscillator (VCO) and a comparison against a reference through a phase-frequency detector (PFD) in a feedback loop configuration. As a result, any change in the natural oscillator frequency due to a change in the tank resonance results in an adaption of the required tuning voltage at the input of the VCO. This dc voltage can be used as the detector output of the sensor. Another concept that has recently been proposed is the use of injection-locked sensing oscillators [63]. An injection-locked oscillator responds to a change of its natural oscillation frequency due to the sensor through a change in its output phase. This phase change can then be converted to a voltage by means of a mixer, driven by a reference [64]. The main drawback of the concept is the need for a high-frequency locking source.

Fig. 6(a) shows an extended concept that allows for a complex readout of a sensing oscillator. Here, a power detector first measures the variation of the amplitude due to the conductivity of the MUT, before a mixer-based frequency
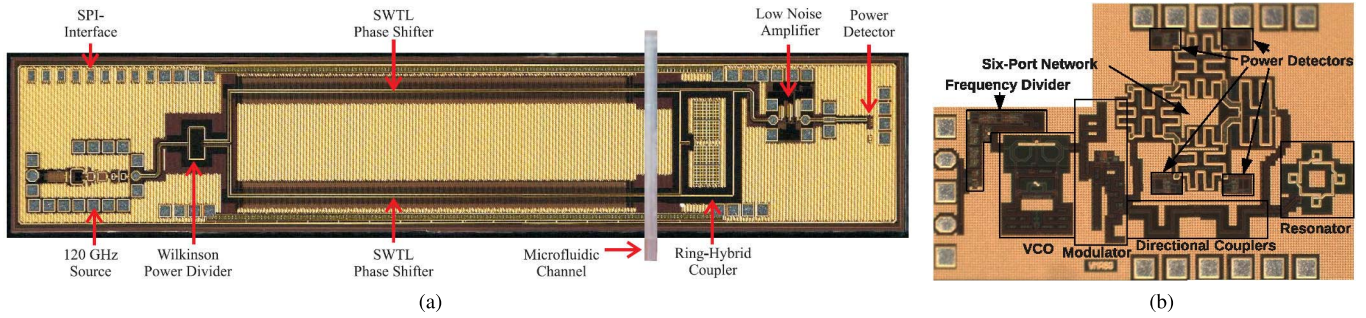
Fig. 7. Chip photographs of (a) integrated 120-GHz interferometric permittivity sensor [66] and (b) 60-GHz six-port reflectometer [67].
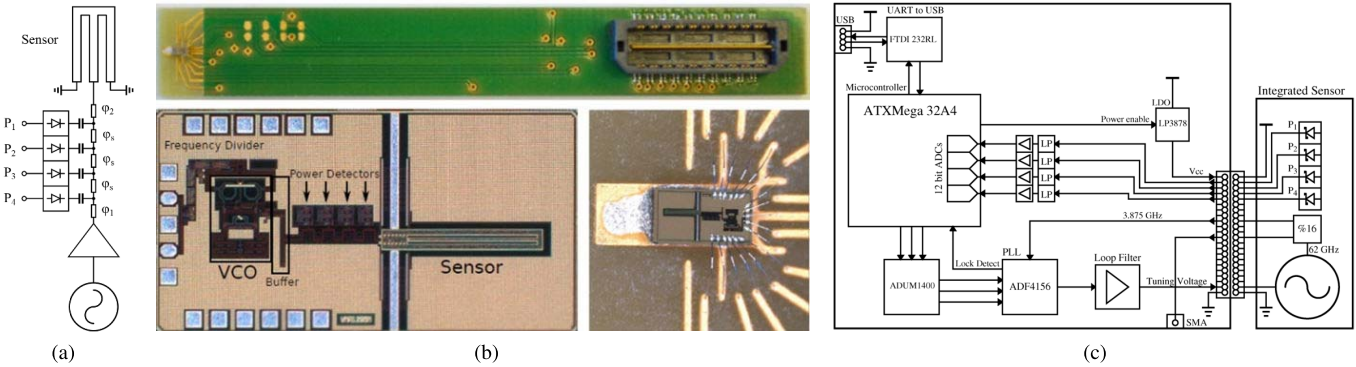
Fig. 8. (a) Concept and (b) chip photograph of a 120-GHz reflectometer with a sampled-line detector. (c) Permittivity sensor demonstrator [68].

discriminator determines the frequency shift, related to the change of the sensor reactance. A buffer, inserted between the power detector and mixer, decouples both detection principles. A fully integrated version of the dielectric sensor, operating at 30 GHz and intended for complex characterization of biological materials, has been demonstrated in [56]. The chip with a size of 2.3 mm^2 and a power consumption of 50 mW is depicted in Fig. 6(b). By embedding multiple such sensors on a single chip, differential measurements can be performed that can cancel out correlated effects, such as environmental noise, temperature, and manufacturing variations [65].

B. Interferometers

While the preceding sensing oscillator approach allows for a low power consumption, it also possesses a number of inherent system limitations due to the cross dependency of amplitude and phase behavior inside the oscillator feedback loop. Therefore, it is useful to decouple the stimulus generation from the sensor interaction, following the principle of Fig. 1(a). To further simplify the measurement, the sensing element can be put into an interferometer configuration, where the stimulus is split into a sensor arm and a reference arm [69]. The idea is to set both the amplitude and phase in the reference arm for a specific frequency in a way that leads to destructive interference when both signals are subsequently recombined. The phase shift and attenuation of the sensor then correspond to the parameters set in the reference path. This output nulling approach works with a simple power detector at the output and also provides advantages for a high impedance range [70].

Fig. 7(a) shows the chip photograph of an electrical interferometer in a 130-nm BiCMOS technology for contactless permittivity measurements operating at 120 GHz [66]. The integrated interferometer is comprised of a 120-GHz VCO with a tuning range of 7 GHz, which acts as the stimulus. A frequency divider chain by 64 is integrated with the VCO to enable stabilization via a PLL. Switchable slow wave transmission lines in each arm act as high-resolution phase shifters, and the output is sensed via a low-noise power detector. A permittivity characterization technique, which includes loading the two microstrip line sensors (reference and measurement channel) and performing the aforementioned phase compensation technique, has been used to successfully determine the dielectric properties of biological samples [71].

An advanced concept of an interferometer is the so-called six port [72]–[74]. The idea behind this structure is the overlay of the received signal with a reference signal at four different phase differences, typically spaced 90° apart from each other to form a differential quadrature set. If the reference and the received signal are of the same magnitude, interferometric mode operation is possible. Otherwise, a strong reference (LO) would result in a differential IQ mixer based on additive mixing at the detectors. An example of an integrated 60-GHz six-port reflectometer is shown in Fig. 7(b) [67]. The meandered six-port network, comprised of hybrids and power dividers, is clearly visible. Through the addition of a 60-GHz VCO and a directional coupler, a highly integrated interferometer has been realized. An optional modulator can serve as a chopper.

The six-port concept of four-phase wave superposition can further be simplified for even higher frequencies. In its
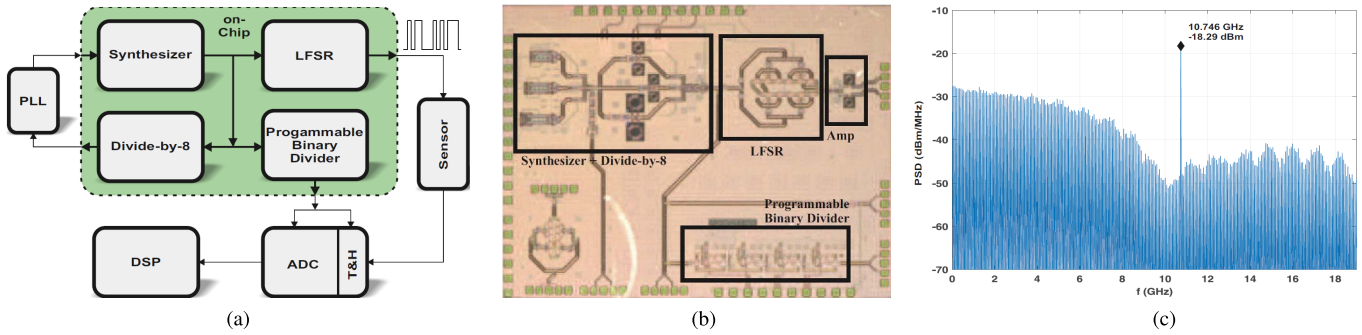
Fig. 9. (a) Block diagram and (b) TX chip photograph with (c) output spectrum of a miniaturized M-sequence-based PRBS sensor system [75].
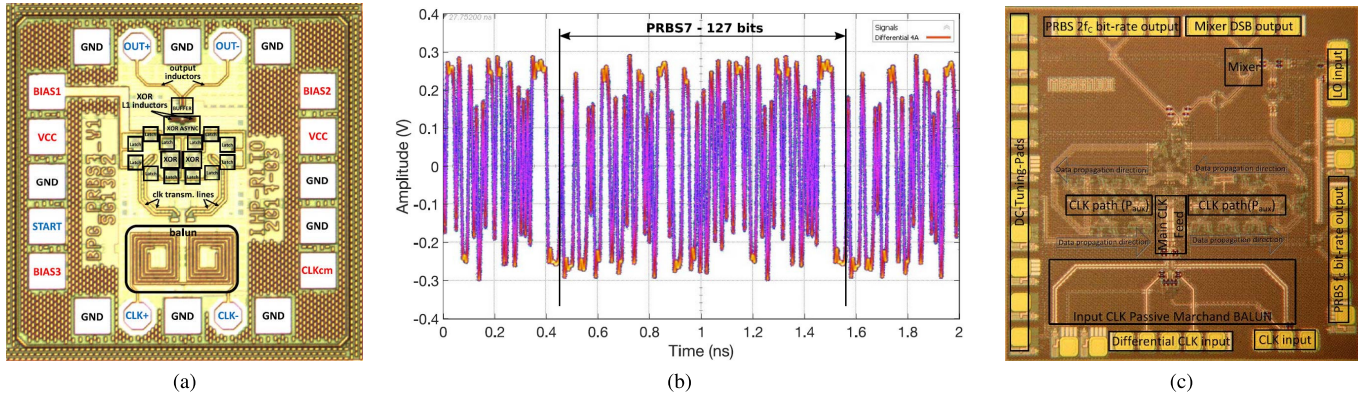
Fig. 10. (a) Chip photograph and (b) output waveform of a 115-Gb/s PRBS generator [76]. (c) Versatile 80-Gb/s, 20–60-GHz PRBS TX [77].

simplest form, the concept features a single transmission line tapped with four sensors at 90° offset after Fig. 8(a). These can sample the standing wave pattern that results from mismatches at the sensor interface, enabling the determination of a reflection coefficient. Fig. 8(b) shows the first fully integrated dielectric biosensor in the millimeter-wave range based on this principle in a 250-nm BiCMOS technology on an area of 1.4 mm² [68]. The sensor consists of a 500-μm shorted half-wavelength coplanar line in the uppermost metal layer. Within a system demonstrator according to Fig. 8(c), the reflectometer is able to measure the reflection coefficient from 118 to 133 GHz.

C. Pseudorandom Sequences

The use of a broadband sensor, such as a transmission line loaded by an MUT, necessitates a stimulus generation and detection with a large bandwidth. The signal generation via a single tunable VCO with low phase noise is typically limited to around 30% [78] but can be pushed to an octave bandwidth through the use of arrays or mixing and multiplication of signals. This approach is especially cumbersome for multioctave microwave bandwidths that extend to very low frequencies. In this case, the use of pseudo-noise techniques can be highly beneficial. Here, quasi-white noise sequences, such as a maximum-length (M) sequence, can be used to characterize the transfer function of a sensor via a Fourier transformation of the cross correlation of the input with the output signal [79], [80]. M-sequences are periodic binary sequences that can conveniently be generated by an n-stage

shift register yielding a sequence of period length $L = 2^n - 1$. Due to the inherent periodicity, subsampling of the output is possible. In addition, it allows the use of fast Hadamard transformations. In principle, the measurement channel (RX) can even be decoupled from the transmitter (TX) completely, when an analog synchronization scheme is used [81].

Chipsets based on M-sequences for ultra-wideband sensing have been presented [82]. In Fig. 9(a), the block diagram of a miniaturized transmission-based M-sequence sensor system is depicted. Here, the pseudorandom binary sequence (PRBS) is generated via an 11-bit linear feedback shift register (LFSR). The clock is generated by an on-chip synthesizer, which is also divided in frequency to supply the subsampling clock to an external ADC with a track-and-hold input. Finally, the impulse response is calculated in the digital signal processing (DSP) unit via a fast M-sequence transformation, which can be converted into the frequency domain by the well-known Fourier approach. Fig. 9(b) shows the corresponding chip photograph of the highly integrated $2^{11} - 1$ PRBS TX for biomedical applications [75] in a 0.35-μm bipolar technology with an area of 12 mm². The TX can generate bit rates up to 10 Gb/s [see Fig. 9(c)], resulting in a minimum bandwidth of 5 GHz if low-pass-filtered at half the clock rate.

The frequency range of operation can further be extended into the millimeter-wave spectrum through the use of high-speed technologies. A state-of-the-art example in 130-nm BiCMOS is shown in Fig. 10(a), which shows the chip photograph of a 7-bit LFSR TX with a bit rate of up to 115 Gb/s [see Fig. 10(b)], a record efficiency of 0.87 pJ/b, and a size of
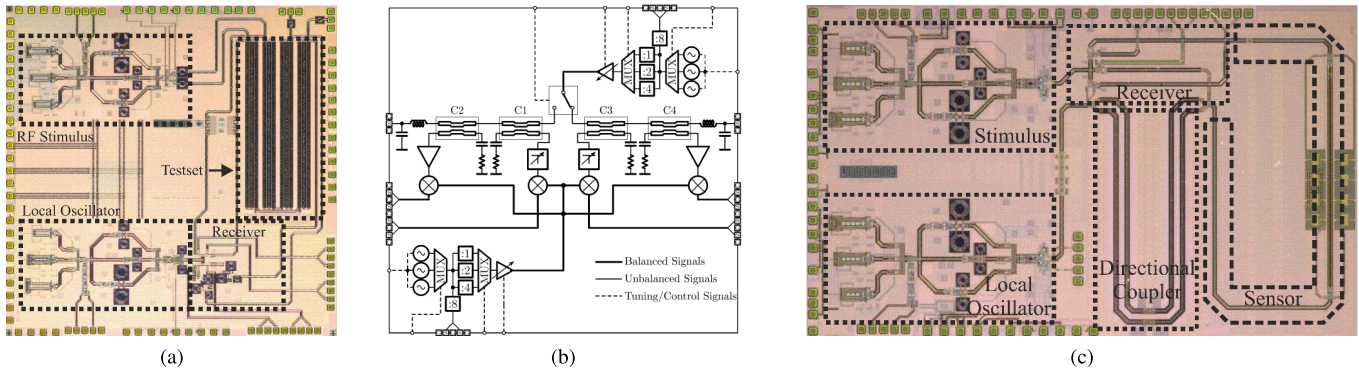
Fig. 11. (a) Photograph and (b) block diagram of an integrated 4–32-GHz heterodyne two-port VNA. (c) Reduced-size VNA with integrated sensor [84].
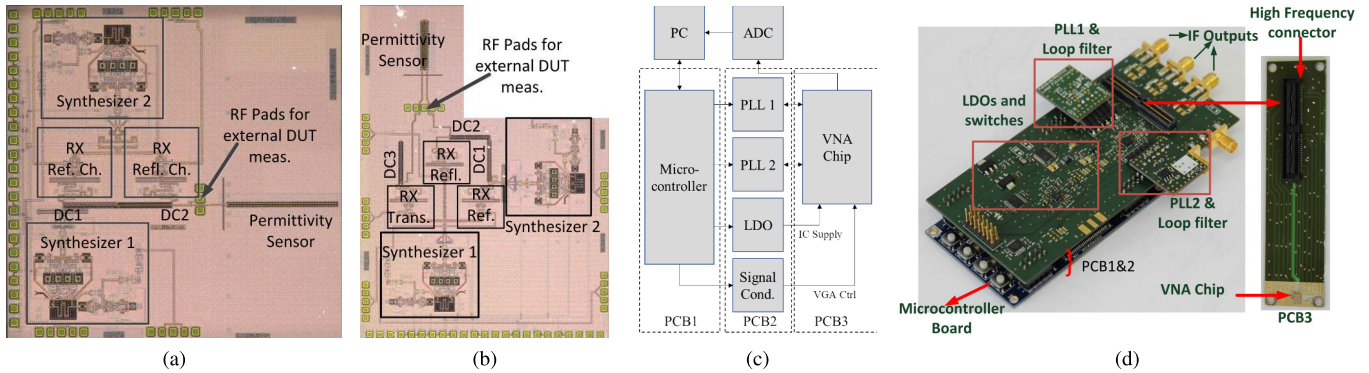
Fig. 12. (a) Reflectometer and (b) two-port version of an integrated 50–100-GHz heterodyne VNA. (c) System block diagram and (d) demonstrator [85].

0.64 mm^2 [76]. To achieve such a high bandwidth, a half-rate topology has been used. An alternative millimeter-wave TX, using a combination of PRBS generation and spectrum shifting via double-sideband mixing, is shown in Fig. 10(c). The TX relies on a number of broadband circuit techniques [83] and realizes a versatile stimulus with an 11-bit, 80-Gb/s PRBS generator whose spectrum can be doubled and centered from 20 to 60 GHz via a broadband mixer [77]. The TX consumes a chip area of 2.25 mm^2 and was manufactured in an 0.35-μm SiGe bipolar technology.

D. Network Analyzers

Over the last ten years, an increased effort has been spent by the research community to integrate certain functions of a network analyzer according to Fig. 3(a) and (b). The motivation behind this is the proliferation of broadband miniaturized high-frequency sensor solutions. In [86], an integrated measurement (receive) channel from 1 to 50 GHz has been presented, which can be operated in a heterodyne configuration by means of a 3-Hz chopper and a subsequent external demodulator. Another integrated heterodyne receive channel operating up to 3 GHz was shown in [87], and a homodyne version based on IQ mixers working up to 10 GHz was introduced in [88]. In the following, an application-specific 27–40-GHz chipset including a TX and a noncoherent self-mixing RX was successfully used in [89], and a single-chip 3.8–4.8-GHz transceiver solution for a homodyne IQ-mixer-based reflectometer (excluding the directional element)

was presented in the context of electron paramagnetic resonance (EPR) spectroscopy [90]. Finally, a reflectometer RX up to 26 GHz [91] and the first broadband heterodyne 4–32-GHz transmit/receive chipset [92] were introduced.

Fig. 11(a) and (b) shows the subsequent successful realization of a highly integrated heterodyne two-port VNA with a broadband performance from 4 to 32 GHz on a single chip. The circuit has been fabricated in a commercial 0.35-μm SiGe bipolar technology and occupies a chip area of 3 × 3 mm^2 [84]. It can be combined with an external passive microwave biosensor to yield a powerful miniaturized sensing system. The chip contains two independent broadband signal sources, realized through a multiplexed oscillator array, which can be locked via a dual PLL architecture. Furthermore, the system contains a set of four directional couplers for wave separation and Gilbert-cell-based downconversion mixers to implement the measurement and reference channels. The presented chip was embedded in a system demonstrator and showed excellent agreement with the results of a commercial VNA (PNA-X) after calibration. In addition, a fully integrated version, depicted in Fig. 11(c), with an on-chip sensor has been realized.

The previously used SiGe bipolar technology with an f_t/f_{max} of 170/250 GHz can support even higher operating frequencies. Consequently, both a highly integrated two-port VNA as well as a reflectometer covering the octave bandwidth of 50–100 GHz have been realized, as shown in Fig. 12(a) and (b) [85]. The circuits are based on the broadband integrated transceiver building blocks, including a
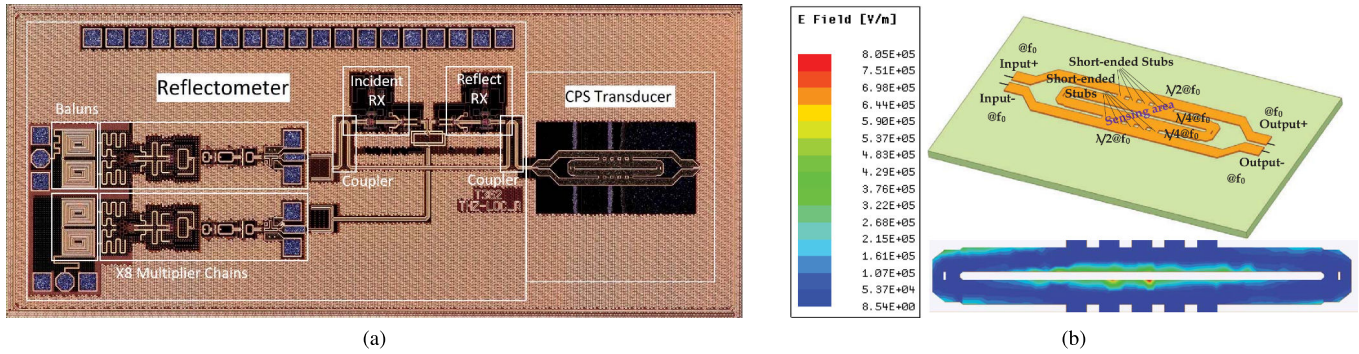
Fig. 13.   (a) Chip photograph of a frequency-extending 200–240-GHz reflectometer-based integrated analyzer and (b) co-integrated resonant sensor [94].
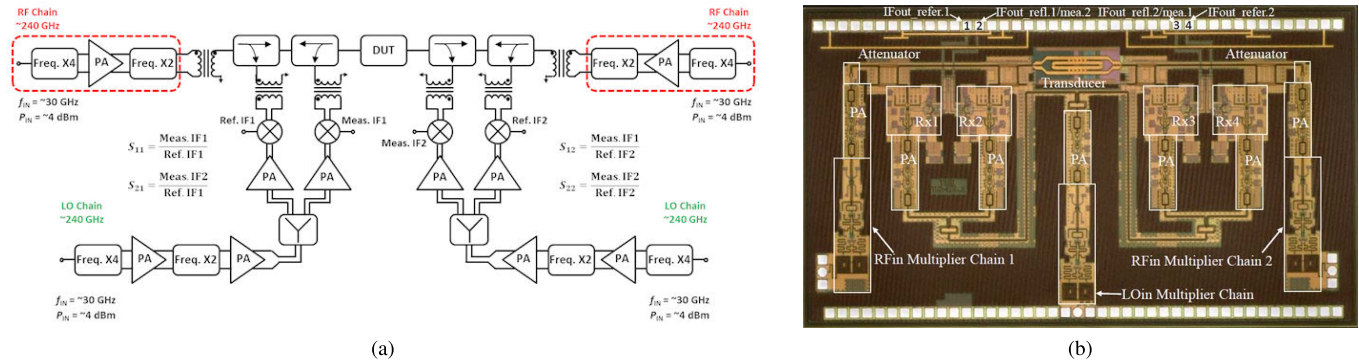
Fig. 14.   (a) Frequency-extending heterodyne two-port analyzer concept and (b) photograph of a 207–257-GHz implementation with three multipliers [95].

single-sideband selecting 50–100-GHz synthesizer, presented in [93]. The aforementioned chips can be used to measure complex scattering parameters of external devices or determine the permittivity of different materials using an integrated dielectric sensor in transmission or stub configuration. Fig. 12(c) shows the measurement system block diagram including the synchronization of the two on-chip synthesizers via an external dual-loop PLL. The resulting modular demonstrator board of the 50–100-GHz VNA, shown in Fig. 12(d), has been used for automated measurements of the permittivity of liquids.

E. THz Frequency Extenders

The realization of signal sources beyond 100 GHz becomes increasingly difficult, due to the transistor gain limitations, high losses in the passive networks, and prohibitively low-quality factors of the tuning elements such as varactors. Therefore, system architectures based on frequency multiplication both for the RF stimulus as well as the LO in the measurement and reference paths are used to achieve broadband target frequencies in the D-band (110–170 GHz) or even higher into the THz regime [96]–[100]. In measurement equipment, the required frequency multipliers, mixers/detectors, and directional couplers are typically outsourced as a so-called frequency extender and combined with a lower-frequency VNA.

Integrating such a frequency extension module into an on-wafer measurement probe is called active probe [101]–[103] and dates back to the last century where chipsets of nonlinear transmission lines in combination with diode

samplers were proposed [104]–[107]. This principle of a frequency extender can readily be adopted for integrated millimeter-wave and THz analyzers. The resulting standalone integrated circuit typically features RF and LO inputs in the microwave-frequency range to limit the on-chip multiplication factor and IF output ports for the measurement and reference channels. Recently reported work in this area includes reflectometers in the W-band (70–110 GHz) [108], [109] and the G-band (160–200 GHz) [110].

In the context of millimeter-wave and THz sensor readout, the frequency extender principle has first been proposed in a transmission-based setup in [111] with a single 215–245-GHz multiplier chain, an integrated resonant sensor, and an IQ-mixer-based complex measurement channel. Fig. 13(a) shows a related realization of an integrated 200–240-GHz heterodyne reflectometer with the aforementioned resonant stripline sensor, visible in Fig. 13(b) in a one-port configuration [94]. Both circuits rely on an advanced 130-nm SiGe BiCMOS technology that features an f_t/f_{max} of 300/500 GHz.

An approach to further increase the characterization capability is illustrated in Fig. 14(a). Here, a full two-port heterodyne VNA architecture is described that uses four dedicated multiplier chains to generate both the stimuli as well as the LO signals for the measurement and reference channels. The most recent result and state of the art in the field, demonstrating the integration capabilities of silicon technology, are shown in Fig. 14(b). The figure depicts a fully integrated frequency-extending two-port VNA that operates from 207 to 257 GHz using a shared multiplier chain for all mixer LO ports. The circuit features fully differential measurement ports as well as

TABLE I
COMPARISON OF ANALYZER PRINCIPLES

Type	Bandwidth	Dynamic Range	Accuracy	Meas. Time	Form Factor	Power Cons.	Features
Sensing Oscillator	−	−	−	++	+++	+++	resonant, arrays possible
Sensing PLL/ILO	−	−	+	+	++	++	resonant, external reference
Interferometer	+	++	++	+	++	++	resonant, direct-conversion
PRBS	+++	+	+	+++	++	+	broadband, digital processing
Network Analyzer	++	+++	+++	−−	−−	−−	broadband, heterodyne
Freq. Extender	++	++	+++	−−	−−−	−−−	broadband, external LO

TABLE II
OVERVIEW OF HIGHLY INTEGRATED MICROWAVE AND MILLIMETER-WAVE READOUT CIRCUITS WITH DC/IF OUTPUT

Ref.	Type	Frequency Range	Dynamic Range (RBW[a])	Standard Dev.	Permittivity Acc.[b]	Chip Area	Power Cons.
[62]	Sensing PLL	0.7–6 GHz	-	0.12%	3.7%	6.25 mm^2	250 mW
[56]	Sensing Oscillator	23–27 GHz	-	-	3.7%	2.3 mm^2	60 mW
[68]	Sampled-Line	118–133 GHz	-	S_{11}: 0.22°	0.7%	1.4 mm^2	250 mW
[66]	Interferometer	117–125 GHz	-	S_{21}: 0.06°	0.1%	8 mm^2	-
[91]	Reflectometer[c]	0.01–26 GHz	RX: 126–132 dB (10 Hz)	-	-	1.8 mm^2	640 mW
[84]	Reflectometer 2-Port VNA	4–32 GHz	44-77 dB (100 kHz) RX: 82-101 dB	S_{11}: 0.0027° S_{21}: 0.012°	0.03% 0.03%	16 mm^2	1900 mW
[85]	Reflectometer 2-Port VNA	50–100 GHz	55-73 dB (100 kHz) RX: 57-73 dB	S_{11}: 0.09° S_{21}: 0.09°	0.45% 0.45%	9 mm^2 12 mm^2	2000 mW 2300 mW
[108]	Extender (Refl.)	70–110 GHz	RX: 110–115 dB (10 Hz)	-	-	5.9 mm^2	440 mW
[113]	Extender (2-Port)	207–257 GHz	-	-	-	11 mm^2	2700 mW

[a]Resolution bandwidth; [b]based on linearized methanol:ethanol mixture measurements; [c]with external LO source

an adaptive power tuning via on-chip variable attenuators on a chip area of 11 mm^2. The chip enables the measurement of not only the transmission parameters but also the reflection parameters of a co-integrated resonant stripline sensor. This enables complex sensing of the dielectric properties of biomaterial in close proximity to the sensor structure.

Current silicon technology is, in principle, capable of operating at even higher frequencies, approaching the terahertz range of above 300 GHz. This is especially true for on-chip sensors that do not require excessive stimulus powers, and, recently, first results in the 480-GHz range have been published [112].

F. Comparison

The different analyzer architectures, discussed in this section, feature different advantages and drawbacks that make their use application-specific. Table I shows a qualitative comparison of the individual analyzer principles against each other. Sensing oscillators, sometimes embedded in a PLL or injection locked to a reference, have an inherent resonant characteristic with a limited dynamic range due to the maximally allowed loss before cease of oscillation. On the other hand, they can be very compact in size with low power consumption and are suitable for 2-D array sensing at millimeter-wave frequencies. Interferometers, including sampled lines, are based on direct-conversion/power detection, which still limits the dynamic range. However, in comparison with oscillators, the passive resonant elements typically provide a wider bandwidth when based on transmission-line techniques. PRBS-based analyzers (for example, based on M-sequences) rely on digital processing techniques. The principle allows for very high relative

bandwidths in the lower microwave spectrum combined with a fast measurement time. At the same time, the achievable signal-to-noise ratios and, hence, the accuracy and dynamic range are limited. VNA and related frequency extender architectures, either realized as one-port reflectometers or two-port systems, can achieve the highest accuracies and dynamic ranges, due to their heterodyne conversion principle combined with a low instantaneous bandwidth. Heterodyning further enables a large bandwidth because of the lack of broadband (IQ) phase shifters in the RF domain. A careful choice of the LO frequency in an extender architecture can lead to optimal phase noise and, hence, accuracy, while penalties in dynamic range, form factor, and power consumption arise from the frequency multiplier.

A more detailed presentation of various published highly integrated analyzers with dc or IF readout with quantitative results is given in Table II. One can clearly observe the trade-off between narrowband low-power and small form factor resonant approaches, such as sensing oscillators, and broadband high-dynamic range and high-accuracy network analyzers with significantly increased area and power consumption. Table II also provides the corresponding linearized (real) permittivity accuracy for the standard methanol:ethanol reference.

Fig. 15 shows an example measurement of such a methanol:ethanol mixture using an integrated 50–100 GHz reflectometer from [85]. Here, the (uncalibrated) phase results are shown, as these typically provide the highest accuracy. On can clearly see the influence of the 50-GHz resonant stub, which increases the phase sensitivity in this frequency range.
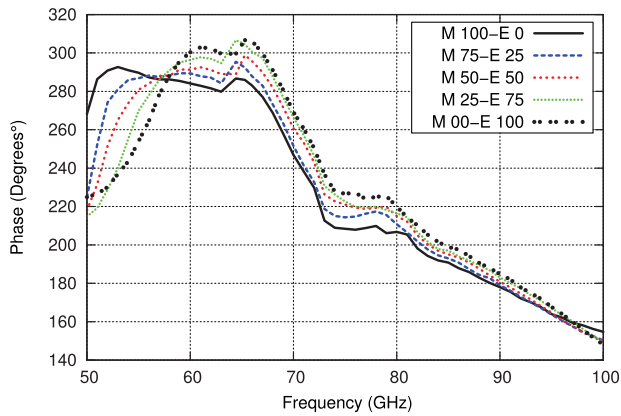
Fig. 15. Example phase measurement of methanol:ethanol mixtures using the reflectometer from [85] in combination with a 50-GHz resonant stub.

IV. SENSOR SYSTEMS

A. Microfluidic Lab-on-Chip Sensors

Due to their short wavelength, millimeter-wave and THz sensors provide the possibility of a contactless, noninvasive, and non-ionizing characterization of geometrically small biological samples, such as molecules, single cells, or cultures. An investigation of cellular properties requires a buffer medium to keep the cells alive, which can mask the cell analysis at frequencies below GHz. In addition, broadband approaches provide a certain potential for a label-free analysis. For this purpose, standalone coplanar sensors have been investigated up to 110 GHz in combination with a polydimethylsiloxane (PDMS) microfluidic channel atop the transmission line [116]–[118], including the use of resonant approaches [119], [120]. It has further been shown that bandpass-type on-chip integrated 120-GHz sensor structures can interact with external microfluidic channels formed by quartz capillaries with ultra-thin walls [121].

Bringing both the high-frequency analyzer-on-a-chip and the microfluidic environment together requires novel advances in micro-fabrication and technology that enable the development of a true high-frequency lab-on-a-chip. Here, nanoliter volumes need to be transported close to the sensor device to enable electromagnetic interaction and cellular characterization. Recently, the first fully BiCMOS integrated micro-channel technology for millimeter-wave and THz biosensing applications has been proposed [114]. Fig. 16(a) shows the principle integration concept of the microfluidic backend into the BiCMOS technology. The process integration is relatively easy and adds only two mask steps to the standard CMOS process to maintain a low-cost approach. One of the advantages of this concept is that the fluidic inlet and outlet are located at the backside of the chip and do not interact with the electrical interfaces on the topside. This fact allows a number of different packaging options for various application scenarios. On the other hand, one of the drawbacks of the presented platform is the need of inlet and outlet interfaces on a geometrically larger higher-level domain. As a result, the fluidic interfaces can be much larger in size than the electrical interfaces, therefore increasing the overall chip area for low-complexity sensors, as shown in the manifold system in Fig. 16(b). Here, a 5×5 mm^2 area is required to fit the chip into the cavity, which self-aligns to the O-rings to prevent any leakage. Fig. 16(c) shows the measurement setup with fluid pumps for velocity and pressure control.

The aforementioned lab-on-chip technology has been applied to a 120-GHz dielectric sensor [122], and measurements have been performed for different fluids to extract the complex dielectric constant [115]. Fig. 17(a) shows the chip photograph of the 120-GHz dielectric sensor with the integrated micro-channel. The BiCMOS microfluidic lab-on-chip generates the 120-GHz test stimulus via an on-chip VCO. The signal passes a resonant transducer, which interacts with the MUT inside the micro-channel, and the resulting high-frequency response of the filter is read out by an on-chip detector. Using this lab-on-chip, permittivity perturbations in fluids inside the co-integrated channel [Fig. 17(b) and (c)] could be detected. Alternative approaches for the integration of the micro-channels include additional oxide deposition in combination with deep reactive ion-etched channels [123].

B. Point-of-Care THz Gas Spectrometers

Rotational gas spectroscopy (RGS) is an emerging application field for millimeter-wave and terahertz integrated sensors. It combines broadband free-space quasi-optical network analysis [125]–[127] with a gas absorption cell. This technique has the critical advantage of high specificity under low pressure. RGS can, for example, be used to provide a stable high-frequency source via locking to an absorption line of a known gas, called a molecular clock [113]. In the field of biomedical systems, one of the most interesting applications is the analysis of exhaled human breath, for example, via the detection of volatile organic compounds [128]. In previous years, a number of publications have shown CMOS transmitter realizations for gas spectroscopy applications in the frequency range from 85 to 180 GHz [129]–[131]. Furthermore, a 220–320-GHz comb spectrometer for the molecular clock was introduced [132].

Fig. 18(a) and (b) shows a 240-GHz chipset comprised of a transmitter array and a RX [124]. It is used within a spectroscopic system in the frequency range from 238 to 252 GHz. The four-element spatial power-combining transmitter array can provide +7 dBm of output power and an effective isotropically radiated power (EIRP) of +18 dBm [133]. Each TX path consists of a two-stage power amplifier, a frequency doubler, and an integrated antenna. These parallel paths are driven by a 120-GHz on-chip push-push LO with a differential amplifier and subsequent Wilkinson power divider. The corresponding RX is based on a subharmonic downconversion mixer concept and an identical LO. The complete system can be stabilized via an external low-frequency PLL by means of the integrated divide-by-64 frequency dividers. To further increase the operating frequency range, it is possible to integrate multiple TX or RX chains with a recentered frequency of operation on a single die. This has been demonstrated in [134] and resulted in an overall operational frequency range of 222–270 GHz.
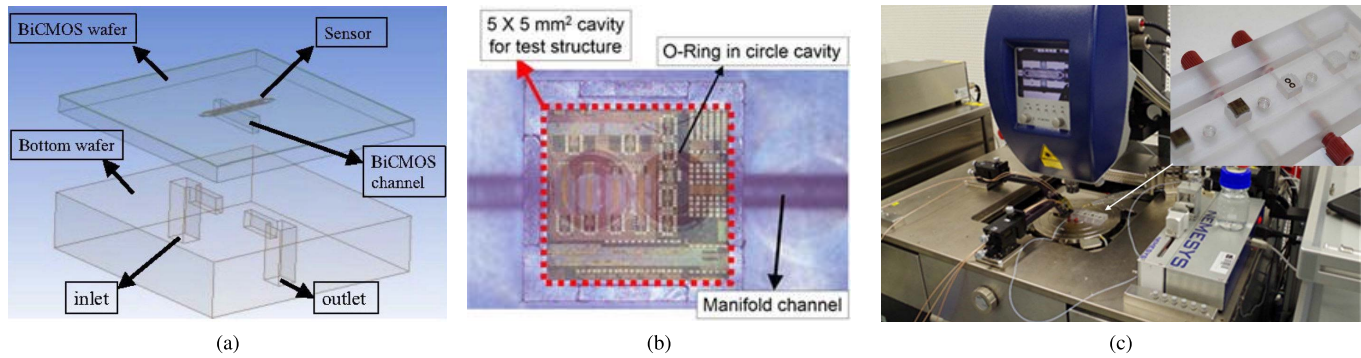
Fig. 16.   (a) Microfluidic integration concept and (b) photograph of the fluidic O-ring interfaces, as well as (c) lab-on-chip measurement setup [114].
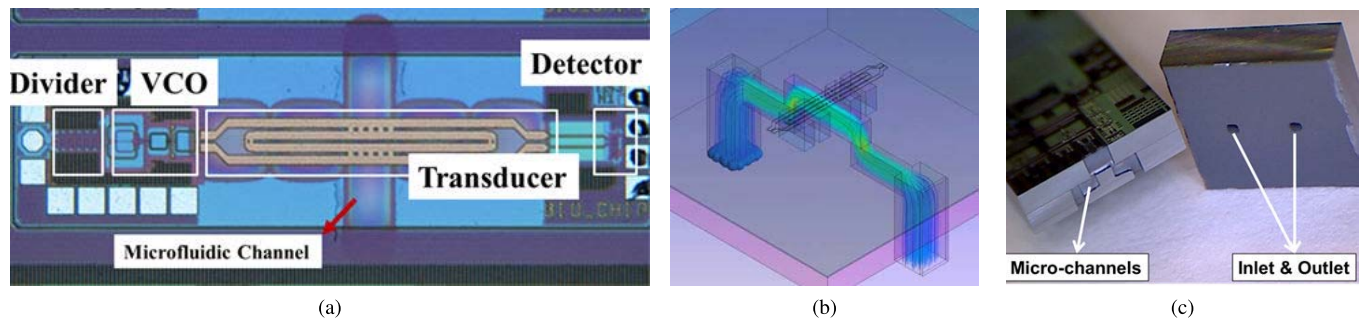
Fig. 17.   (a) 120-GHz microfluidic lab-on-a-chip sensor and (b) flow simulation, as well as (c) physical realization of the microfluidic channels [115].

Today's integrated circuit technology allows for the realization of circuits for even higher spectral analysis. In Fig. 18(c) and (d), an example of a spectroscopic transmit/receive chipset at 500 GHz is depicted [135]. The 500-GHz transmitter array includes a frequency quadrupler instead of the previously implemented doublers and consumes a total chip area of 8.6 mm^2. For the 500-GHz RX, a frequency doubler to 500 GHz is inserted between the 125-GHz LO and a transconductance subharmonic mixer. The die area of the fabricated RX chip is 2.1 mm^2. Recently, these chipsets have been further improved, covering 440–540 GHz [136], [137].

Various gas spectroscopy systems have been realized based on the abovementioned chipsets, either by direct tuning [138] or by operation inside a PLL. Fig. 19(a) shows an example of the latter. The spectroscopic system includes a gas absorption cell [124] shown in Fig. 19(a), with a length of 0.6–1.9 m. A frequency modulation at the TX enables the determination of the second harmonic content (2f) of the absorption spectrum by means of an IF lock-in amplifier. Fig. 19(c) shows the 2f absorption spectrum of a gas mixture of CH_3OH and CH_3CN at a pressure of 11 Pa around 500 GHz. Excellent agreement to the integrated NASA Jet Propulsion Laboratory (JPL) absorption coefficients is observable.

C. Invasive and Implanted Sensors

A number of invasive medical applications for microwave- and millimeter-wave sensors have been discussed. One of them is the integration of such high-frequency sensors into catheter tips for the diagnosis of arteriosclerosis. Here, these sensors can be used to detect plaque formation in arterial vessels based on the associated dielectric contrast and even, more importantly, can distinguish between different (fibrous white and high-cholesterol yellow) plaque types. The realization of such a sensor solution in a clinical environment necessitates appropriate integration and packaging techniques [141]. Moreover, the sensing concept needs to ensure non-contact operation due to the risk of plaque release in an intra vascular measurement, which can cause embolism.

A millimeter-wave sensing concept, based on an integrated circuit operating at 30 GHz and a matching transmit/receive antenna pair, has been proposed in [142]. The chip contains a signal source for radiation of the stimulus via the antenna and an IQ RX to detect the amplitude and phase of the reflected signal. In the concrete scenario, the received signal is a multipath combination of direct antenna coupling, mismatches, and the (desired) reflection at the blood-to-arterial wall interface. An alternative concept is presented in Fig. 20(a) and (b) [139]. The sensor is based on a 27-GHz sensing oscillator with an electromagnetically exposed microstrip stub line inside the resonant tank. The resulting frequency change due to a change in the permittivity of the MUT in proximity to the transmission line is detected via an on-chip frequency discriminator, similar to the architecture in Fig. 6(a). The chip is mounted on a long flexible polyimide interposer with a width of 1.2 mm and a thickness of 0.2 mm. Because of this minimal size, the interposer could be combined with an 8F (French gauge system, 3F equals 1 mm) diameter catheter suitable for further clinical use in cardiology and heart surgery. *Ex vivo* results of the detection of plaque formation in human tissue with a first sensor version are shown in Fig. 20(c). Fig. 20(a) shows the results for healthy tissue that yields an output voltage of 0.5 V, while the calcified
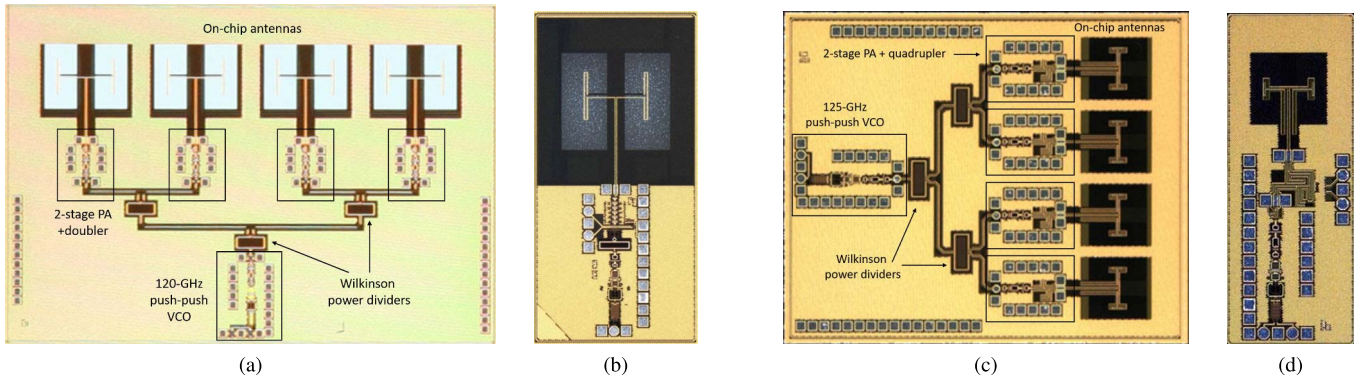
Fig. 18.   Chip photographs of a 240-GHz (a) transmitter array and (b) RX, as well as a 500-GHz (c) transmitter array and (d) RX [124].
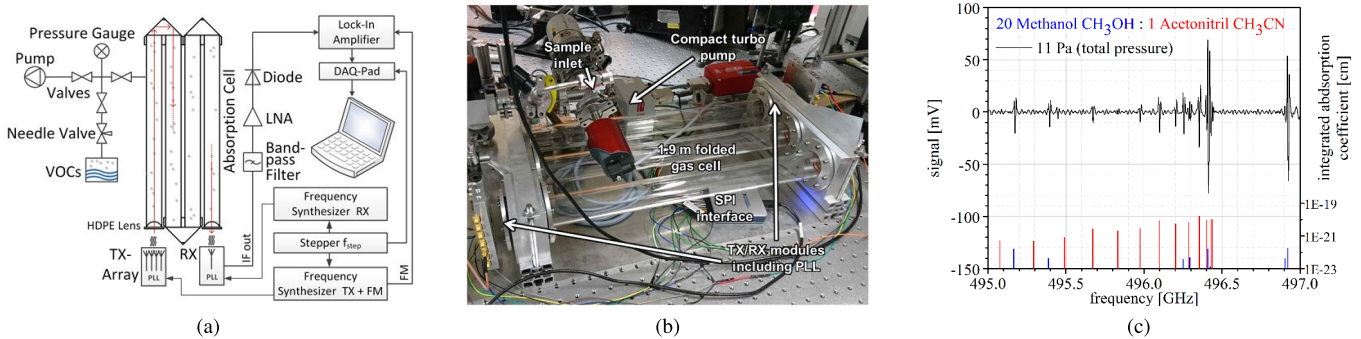
Fig. 19.   (a) System block diagram and (b) gas absorption cell of the spectroscopy measurement setup. (c) 2f absorption spectrum around 500 GHz [124].

pathological tissue of Fig. 20(b) yielded a significantly higher level above 1.7 V.

The encouraging results from the abovementioned experiments have led to an implementation of a high-frequency K-band permittivity sensor in a commercial 130-nm BiCMOS technology [140] for wider application in the detection of biomaterials. Fig. 21(a) shows a block diagram of the integrated system, which contains several enhancements over the previous concept. For example, it resolves the inherent trade-off between the sensitivity to ϵ'-variations and the oscillator tuning range by means of magnetic tuning of the tank inductor. Also, the measurement of the amplitude level of the oscillation via a power detector enables determining both real and imaginary parts of the permittivity. The final chip, shown in Fig. 21(b), consumes 36 mW from a 1.5-V supply and occupies a die area of 1.8 mm^2. Based on this IC, an 18 × 14-mm system-on-board for the fully autonomous implantable continuous monitoring of biomaterials has been realized [143]. It includes a ball-grid array packaged chip, two of the aforementioned 24-GHz complex sensing oscillators, a temperature sensor, wakeup timer, serial-peripheral interface, ADC, and a finite state machine. The latter is used to activate the sensor every 9 min to perform a 4-ms measurement and transmit the data via an integrated 60-GHz TX with in-package antenna.

V. More-Than-Moore Platforms

A. Multimodal Sensing

The microfluidic integration approach presented in the previous chapter can be regarded as a first step toward an application. However, further important aspects need to be considered for a successful commercialization. These include the realization of microfluidic control elements, such as micro-heaters for a defined temperature of the medium, integrated flow meters, as well as trapping electrodes for the separation and fixation of single cells at the sensor. While main considerations such as the localization of inlet and outlet on the backside of the chip for a reduced chip area and simultaneous electrical and mechanical contact have already been considered, the need of practitioners for a simultaneous optical inspection has not been addressed. To enable such a system, a modified three-wafer stack approach, including a glass wafer after Fig. 22(a), has been proposed [144]. In Fig. 22(b), the cross section of the complete integrated BiCMOS microfluidics technology can be seen. Again, the fluids can be fed into the system by a multipurpose manifold, which connects the chip to the pumps and other external fluidic equipment. The concept allows for a simultaneous electrical and optical measurement at the top.

The manufacturing process is based on 200-mm wafer-to-wafer bonding techniques. A single fully processed BiCMOS wafer is used for the integrated electronics, including the stimulus, sensor, and readout circuitry. Meanwhile, the microfluidic channels are etched into a second bare silicon wafer, which is aligned with the former and bonded using plasma-active oxide–oxide fusion bonding. This results in the formation and encapsulation of the microfluidic network at the interface of these two wafers. Then, the channel wafer is grinded from the backside until the pads and channels are exposed. Finally, the glass wafer is bonded on top of the channels by adhesive, and the channels are encapsulated. Once again, the
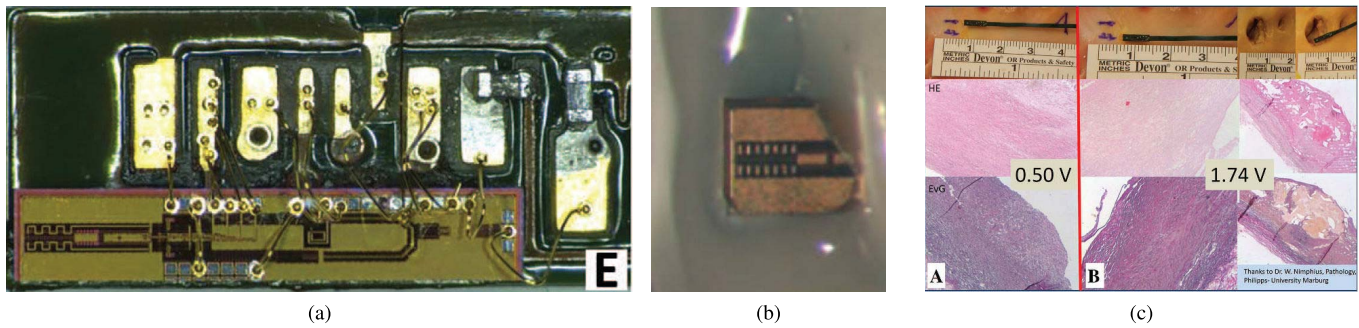
Fig. 20. (a) Photograph and (b) catheter tip packaging of a 27-GHz sensor for intra vascular plaque detection with (c) *ex vivo* results [139].
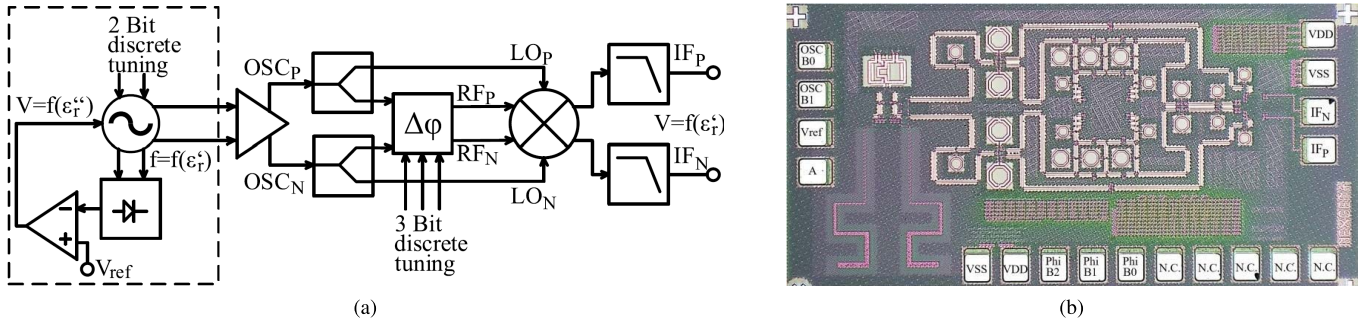
Fig. 21. (a) Block diagram and (b) chip photograph of an integrated implantable 24-GHz biosensor with complex permittivity detection capability [140].

electrical pads have to be cleared, which is done by two-step dicing on the final chips. Fig. 22(c) shows an image of the cross section of the process. The described wafer-bonding approach for a highly integrated millimeter wave or THz lab-on-chip in silicon is most suitable for applications with mass market capability, and a high number of units shipped per year. This can, for example, be a low-cost replaceable sensor module inside a medical or pharmaceutical cartridge. Another promising technology that can be combined with integrated high-frequency analyzers is flexible microfluidics [145].

B. Sensor Functionalization

While gas spectroscopy under low pressure can be used for a finger-print-like identification of constituents, the problem of identification of complex mixtures and compositions in liquid- and solid-state media is significantly more difficult. For example, biological materials, such as tissue and protein solutions, contain a high percentage of water (70%–80%), and the overall behavior is governed by the dielectric properties of water. Essentially, the MUT behaves like a water macro-molecule whose frequency response is perturbed in the presence of additional components. A quantitative determination of these components of interest generally requires additional knowledge and is often limited to binary mixtures. The use of terahertz radiation with distinct molecular resonances potentially provides new opportunities for a better identification in complex media, but the additional presence of secondary signatures, such as surface effects, hinders an effective detection scheme. Furthermore, to increase the sensitivity of a system, intentional geometrical resonances often have to be introduced into a millimeter-wave or terahertz sensor system.

To overcome the abovementioned problems, robust methods for sensor functionalization with a specific response to a desired analyte are highly desirable. Fig. 23(a) shows a free-space large-aperture resonator array readout concept where the terahertz split-ring resonators have been functionalized by an aptamer specific to human African trypanosomiasis, a highly dangerous tropical disease [146]. In Fig. 23(b), the sensor surface with a trypanosome parasite cell coating is shown. The combination of miniaturized high-frequency sensors with such functionalizations will be one key to reliable biomedical applications.

A promising concept that allows functionalized multimodal sensing in the high frequency as well as the optical domain is illustrated in Fig. 24 [147]. Fig. 24 shows a schematic cross section of a CMOS back-end-of-line where a locally applied backside-etching technique followed by a chemical wet etch is used to expose the optical slot waveguide [148]. The overall process steps are fully compatible with a photonic integrated circuit (PIC) technology and allow the deposition of organic materials onto the optical sensor for direct label-free biosensing or dedicated functionalization for a target analyte. For this purpose, a hybrid optical resonator based on the combination of a stripline and a slot-waveguide for functionalized biosensing has recently been demonstrated [149]. As a next step, the presented approach can be combined with a high-performance BiCMOS electronic-PIC (EPIC) technology [150]. In addition to these optical elements, the abovementioned EPIC technology also features high-frequency bipolar transistors, which can pave the way for future monolithic electro-optical multimodal sensor platforms [151] at an unprecedented degree of integration and functionality.
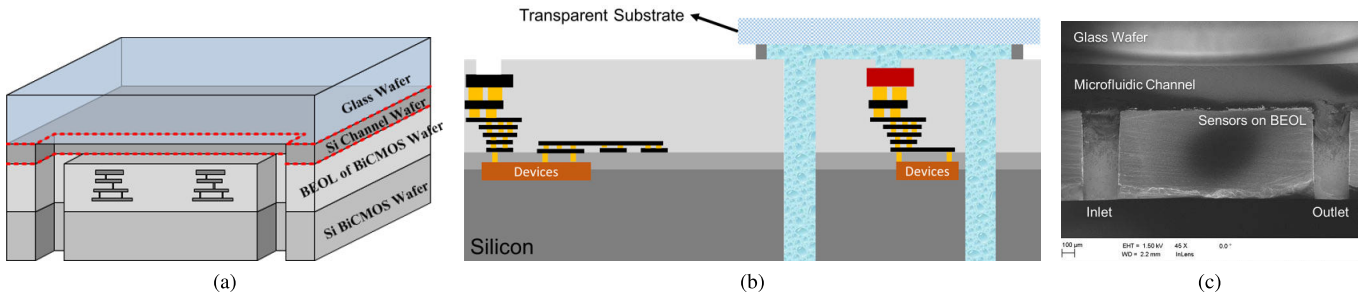
Fig. 22.   (a) Integration approach, (b) schematic BiCMOS microfluidic cross section, and (c) image of the processed lab-on-chip cross section [144].
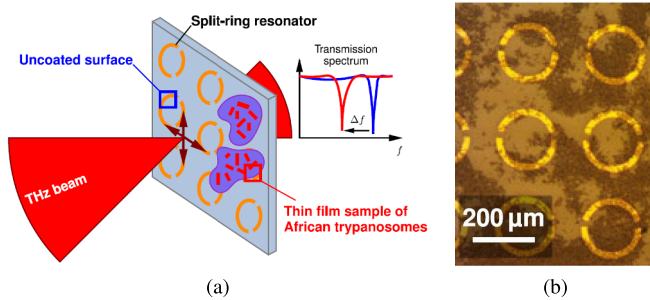
Fig. 23.   (a) Free-space split-ring resonator-array readout concept and (b) sensor coating with parasite of an aptamer-functionalized large-aperture terahertz sensor for African tripanosomes detection [146].
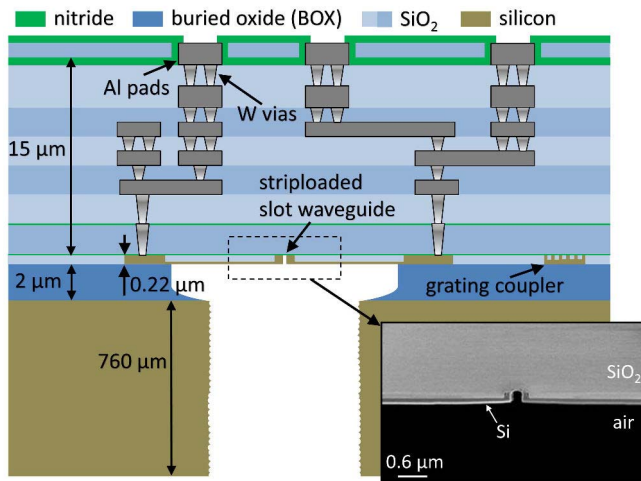
Fig. 24.   Schematic cross section of a CMOS-compatible back-end-of-line with a backside release process for exposure of integrated optical waveguides with a scanning electron microscope image of the optical sensor device [147].

VI. FUTURE DIRECTIONS

Current millimeter-wave and terahertz biosensor realizations still suffer from a number of drawbacks that often hinder their practical application. Among them, the most important is a limited sensitivity or dynamic range, high power consumption, and limited calibration possibilities and stability over longer measurement intervals, and finally cost and throughput. The sensitivity is directly linked to the phase noise of the stimulus plus the added noise of integrated components of the analyzer. For the dynamic range, the linearity of the measurement channels (RX) is of additional importance. The design space

for an optimal dynamic range has already been very well investigated in the context of wireline or wireless systems. It is generally agreed upon that improvements can mainly be achieved through the use of technologies of higher performance (f_t/f_{max}, NF_{min}), such as [19]. This directly results in a lower noise and possible linearity improvements when traded against additional gain via feedback. Furthermore, this allows for a further reduction of the power consumption, which is especially important to allow co-integration of the thermally sensitive sensor element. In addition, such power scaling will enable the simultaneous integration of an increased number of channels on a single chip to bring down cost and improve calibration capabilities and measurement throughput.

VII. CONCLUSION

In this invited paper, the evolution and status of integrated millimeter-wave and terahertz analyzers in silicon technologies have been reviewed. During the last decade, major research advancements have been made that have led to state-of-the-art complex and powerful miniaturized circuit solutions, such as compact VNAs with octave bandwidths and terahertz integrated chipsets for a biomedical gas spectroscopy of up to 500 GHz. Recent breakthroughs in the proliferation of silicon technologies with an f_{max} of 700 GHz will foster novel sensor applications and implementations reaching the 1-THz barrier. In addition, this will enable a drastic improvement in power consumption and stability of millimeter-wave systems. Finally, emerging heterogeneous integration and sensor functionalization approaches will offer new possibilities for reliable, sensitive, and specific biomedical sensor solutions.

REFERENCES

[1] M. Hofmann, G. Fischer, R. Weigel, and D. Kissinger, "Microwave-based noninvasive concentration measurements for biomedical applications," *IEEE Trans. Microw. Theory Techn.*, vol. 61, no. 5, pp. 2195–2204, May 2013.

[2] C. Li, V. M. Lubecke, O. Boric-Lubecke, and J. Lin, "A review on recent advances in Doppler radar sensors for noncontact healthcare monitoring," *IEEE Trans. Microw. Theory Techn.*, vol. 61, no. 5, pp. 2046–2060, May 2013.

[3] P. Hillger, J. Grzyb, R. Jain, and U. R. Pfeiffer, "Terahertz imaging and sensing applications with silicon-based technologies," *IEEE Trans. THz Sci. Technol.*, vol. 9, no. 1, pp. 1–19, Jan. 2019.

[4] K. Grenier *et al.*, "Recent advances in microwave-based dielectric spectroscopy at the cellular level for cancer investigations," *IEEE Trans. Microw. Theory Techn.*, vol. 61, no. 5, pp. 2023–2030, May 2013.

[5] Y. Ning *et al.*, "Broadband electrical detection of individual biological cells," *IEEE Trans. Microw. Theory Techn.*, vol. 62, no. 9, pp. 1905–1911, Sep. 2014.

[6] F. Artis *et al.*, "Microwaving biological cells: Intracellular analysis with microwave dielectric spectroscopy," *IEEE Microw. Mag.*, vol. 16, no. 4, pp. 87–96, May 2015.

[7] X. Ma, X. Du, H. Li, X. Cheng, and J. C. M. Hwang, "Ultra-wideband impedance spectroscopy of a live biological cell," *IEEE Trans. Microw. Theory Techn.*, vol. 66, no. 8, pp. 3690–3696, Aug. 2018.

[8] M. Hofmann, T. Fersch, R. Weigel, G. Fischer, and D. Kissinger, "A novel approach to non-invasive blood glucose measurement based on RF transmission," in *Proc. IEEE Int. Symp. Med. Meas. Appl.*, Bari, Italy, May 2011, pp. 39–42.

[9] M. Hofmann, M. Bloss, R. Weigel, G. Fischer, and D. Kissinger, "Non-invasive glucose monitoring using open electromagnetic waveguides," in *Proc. 42nd Eur. Microw. Conf.*, Amsterdam, The Netherlands, Oct. 2012, pp. 546–549.

[10] H. Choi *et al.*, "Design and *in vitro* interference test of microwave noninvasive blood glucose monitoring sensor," *IEEE Trans. Microw. Theory Techn.*, vol. 63, no. 10, pp. 3016–3025, Oct. 2015.

[11] P. H. Siegel, A. Tang, R. Kim, G. Virbila, F. Chang, and V. Pikov, "Noninvasive *in vivo* millimeter-wave measurements of glucose: First results in human subjects," in *Proc. 42nd Int. Conf. Infr., Millim., THz Waves (IRMMW-THz)*, Cancun, Mexico, Aug. 2017, pp. 1–2.

[12] A. Moreno-Oyervides, M. C. Aguilera-Morillo, F. Larcher, V. Krozer, and P. Acedo, "Advanced statistical techniques for noninvasive hyper-glycemic states detection in mice using millimeter-wave spectroscopy," *IEEE Trans. THz Sci. Technol.*, vol. 10, no. 3, pp. 237–245, May 2020.

[13] F. Topfer and J. Oberhammer, "Millimeter-wave tissue diagnosis: The most promising fields for medical applications," *IEEE Microw. Mag.*, vol. 16, no. 4, pp. 97–113, May 2015.

[14] F. Trenz, R. Weigel, and D. Kissinger, "Evaluation of a reflection based dehydration sensing method for wristwatch integration," in *Proc. 21st Int. Conf. Microw., Radar Wireless Commun. (MIKON)*, Krakow, Poland, May 2016, pp. 1–3.

[15] U. R. Pfeiffer *et al.*, "*Ex vivo* breast tumor identification: Advances toward a silicon-based terahertz near-field imaging sensor," *IEEE Microw. Mag.*, vol. 20, no. 9, pp. 32–46, Sep. 2019.

[16] C. Weisenstein, M. Schmeck, D. Schaar, A. K. Wigger, A. K. Bosserhoff, and P. H. Bolivar, "Quantification of dsDNA functionalization efficiency in THz biosensors," in *Proc. 44th Int. Conf. Infr., Millim., THz Waves (IRMMW-THz)*, Paris, France, Sep. 2019, pp. 1–2.

[17] K. A. Baksheeva *et al.*, "The sub-THz emission of the human body under physiological stress," *IEEE Trans. THz Sci. Technol.*, vol. 11, no. 4, pp. 381–388, Jul. 2021.

[18] G. Guarin, M. Hofmann, J. Nehring, R. Weigel, G. Fischer, and D. Kissinger, "Miniature microwave biosensors," *IEEE Microw. Mag.*, vol. 16, no. 4, pp. 71–86, May 2015.

[19] B. Heinemann *et al.*, "SiGe HBT with f$_T$/f$_{max}$ of 505 GHz/720 GHz," in *IEDM*, San Francisco, CA, USA, Dec. 2016, pp. 1–4.

[20] E. Kasper, D. Kissinger, P. Russer, and R. Weigel, "High speeds in a single chip," *IEEE Microw. Mag.*, vol. 10, no. 7, pp. 28–33, Dec. 2009.

[21] D. Kissinger, B. Laemmle, L. Maurer, and R. Weigel, "Integrated test for silicon front ends," *IEEE Microw. Mag.*, vol. 11, no. 3, pp. 87–94, May 2010.

[22] D. Kissinger, R. Agethen, and R. Weigel, "A versatile built-in test architecture for integrated millimeter-wave radar receiver front-ends," in *Proc. IEEE Instrum. Meas. Tech. Conf.*, Graz, Austria, May 2012, pp. 254–258.

[23] K. Yau, E. Dacquay, I. Sarkas, and S. Voinigescu, "Device and IC characterization above 100 GHz," *IEEE Microw. Mag.*, vol. 13, no. 1, pp. 30–54, Jan. 2012.

[24] K. Entesari, A. A. Helmy, and M. Moslehi-Bajestan, "Integrated systems for biomedical applications: Silicon-based RF/microwave dielectric spectroscopy and sensing," *IEEE Microw. Mag.*, vol. 18, no. 5, pp. 57–72, Jun. 2017.

[25] D. Kissinger, G. Kahmen, and R. Weigel, "Millimeter-wave and terahertz transceivers in SiGe BiCMOS technologies," *IEEE Trans. Microw. Theory Techn.*, vol. 69, no. 10, pp. 4541–4560, Oct. 2021.

[26] H. Rücker *et al.*, "A 0.13 μm SiGe BiCMOS technology featuring fT/fmax of 240/330 ghz and gate delays below 3 ps," *IEEE J. Solid-State Circuits*, vol. 45, no. 9, pp. 1678–1686, Sep. 2010.

[27] U. Schwerthoeffer, R. Weigel, and D. Kissinger, "A highly sensitive glucose biosensor based on a microstrip ring resonator," in *IEEE MTT-S Int. Microw. Symp. Dig.*, Singapore, Dec. 2013, pp. 1–3.

[28] J. Grzyb, B. Heinemann, and U. R. Pfeiffer, "A 0.55 THz near-field sensor with a μm-range lateral resolution fully integrated in 130 nm SiGe BiCMOS," *IEEE J. Solid-State Circuits*, vol. 51, no. 12, pp. 3063–3077, Dec. 2016.

[29] B. Yu *et al.*, "Ring-resonator-based sub-thz dielectric sensor," *IEEE Microw. Wireless Compon. Lett.*, vol. 28, no. 11, pp. 969–971, Nov. 2018.

[30] U. Schwerthoeffer, R. Weigel, and D. Kissinger, "Microwave sensor for precise permittivity characterization of liquids used for aqueous glucose detection in medical applications," in *Proc. German Microw. Conf. (GeMiC)*, Aachen, Germany, Mar. 2014, pp. 1–2.

[31] R. K. Yadav, J. Wessel, and D. Kissinger, "A 60 GHz ring sensor with differential feed-lines for dielectric spectroscopy in biomedical applications," in *Proc. IEEE Radio Wireless Symp. (RWS)*, Orlando, FL, USA, Jan. 2019, pp. 1–3.

[32] D. Kissinger *et al.*, "Integrated test concepts for *in-situ* millimeter-wave device characterization," in *Proc. IEEE 13th Int. New Circuits Syst. Conf. (NEWCAS)*, Grenoble, France, Jun. 2015, pp. 1–4.

[33] A. Rumiantsev and N. Ridler, "VNA calibration," *IEEE Microw. Mag.*, vol. 9, no. 3, pp. 86–99, Jun. 2008.

[34] M. Seelmann-Eggebert *et al.*, "On the accurate measurement and calibration of S-parameters for millimeter wavelengths and beyond," *IEEE Trans. Microw. Theory Techn.*, vol. 63, no. 7, pp. 2335–2342, Jul. 2015.

[35] J. Campion and J. Oberhammer, "Silicon micromachined waveguide calibration standards for terahertz metrology," *IEEE Trans. Microw. Theory Techn.*, vol. 69, no. 8, pp. 3927–3942, Aug. 2021.

[36] L. Xie *et al.*, "Electronic calibration for submillimeter-wave on-wafer scattering parameter measurements using Schottky diodes," *IEEE Trans. THz Sci. Technol.*, vol. 10, no. 6, pp. 583–592, Nov. 2020.

[37] X. Ma *et al.*, "A multistate single-connection calibration for microwave microfluidics," *IEEE Trans. Microw. Theory Techn.*, vol. 66, no. 2, pp. 1099–1107, Feb. 2018.

[38] D. Kissinger, B. Laemmle, I. Nasr, and R. Weigel, "Millimeter-wave integrated reflectometer architectures for biomedical applications," in *Proc. IEEE Topical Conf. Biomed. Wireless Technol., Netw., Sens. Syst.*, Austin, TX, USA, Jan. 2013, pp. 61–63.

[39] M. Hiebel, *Fundamentals of Vector Network Analysis*. Munich, Germany: Rohde & Schwarz, 2011.

[40] A. A. Helmy and K. Entesari, "A 1–8-GHz miniaturized spectroscopy system for permittivity detection and mixture characterization of organic chemicals," *IEEE Trans. Microw. Theory Techn.*, vol. 60, no. 12, pp. 4157–4170, Dec. 2012.

[41] K. Kim, N. Kim, S.-H. Hwang, Y.-K. Kim, and Y. Kwon, "A Miniaturized broadband multi-state reflectometer integrated on a silicon MEMS probe for complex permittivity measurement of biological material," *IEEE Trans. Microw. Theory Techn.*, vol. 61, no. 5, pp. 2205–2214, May 2013.

[42] M. Hofmann, J. Nehring, R. Weigel, G. Fischer, and D. Kissinger, "A wideband scalar network analyzer for biomedical dehydration measurements," in *Proc. 35th Annu. Int. Conf. IEEE Eng. Med. Biol. Soc. (EMBC)*, Osaka, Japan, Jul. 2013, pp. 4050–4053.

[43] R. K. Yadav, M. H. Eissa, J. Wessel, and D. Kissinger, "A 60 GHz mixer-based reflectometer in 130 nm SiGe BiCMOS technology toward dielectric spectroscopy in medical applications," in *Proc. IEEE Int. Microw. Biomed. Conf. (IMBioC)*, Philadelphia, PA, USA, Jun. 2018, pp. 88–90.

[44] J. Nehring, I. Nasr, K. Borutta, R. Weigel, and D. Kissinger, "A silicon integrated microwave vector network analyzer for biomedical sensor read-out applications," in *IEEE MTT-S Int. Microw. Symp. Dig.*, Tampa, FL, USA, Jun. 2014, pp. 1–4.

[45] A. A. Helmy, S. Kabiri, M. M. Bajestan, and K. Entesari, "Complex permittivity detection of organic chemicals and mixtures using a 0.5–3-GHz miniaturized spectroscopy system," *IEEE Trans. Microw. Theory Techn.*, vol. 61, no. 12, pp. 4646–4659, Dec. 2013.

[46] R. K. Yadav, J. Wessel, M. H. Eissa, F. I. Jamal, M. Kucharski, and D. Kissinger, "A 30 GHz power detector based reflectometer in 130 nm SiGe BiCMOS for dielectric spectroscopy," in *Proc. IEEE Int. Symp. Circuits Syst. (ISCAS)*, Florence, Italy, May 2018, pp. 1–4.

[47] M. Hofmann, A. Oborovski, R. Weigel, G. Fischer, and D. Kissinger, "A microwave VNA for biomedical in-line concentration measurements," in *Proc. IEEE Topical Conf. Biomed. Wireless Technol., Netw., Sens. Syst.*, Austin, TX, USA, Jan. 2013, pp. 46–48.

[48] A. Koelpin, G. Vinci, B. Laemmle, D. Kissinger, and R. Weigel, "The six-port in modern society," *IEEE Microw. Mag.*, vol. 11, no. 7, pp. 35–43, Dec. 2010.

[49] M. Hofmann, F. Trenz, R. Weigel, G. Fischer, and D. Kissinger, "A microwave sensing system for aqueous concentration measurements based on a microwave reflectometer," in *IEEE MTT-S Int. Microw. Symp. Dig.*, Montreal, QC, Canada, Jun. 2012, pp. 1–3.

[50] F. Trenz, M. Hofmann, R. Weigel, and D. Kissinger, "A broadband 3–29 GHz reflectometer with a frequency compensated multilayer sixport structure," in *Proc. Eur. Microw. Conf. (EuMC)*, Paris, France, Sep. 2015, pp. 323–326.

[51] A. Bauch, M. Hofmann, J. Nehring, R. Weigel, and D. Kissinger, "A 2–30 GHz multi-octave planar microwave six-port for reflectometry applications," in *Proc. Eur. Microw. Conf. (EuMC)*, Paris, France, Sep. 2015, pp. 52–55.

[52] M. Hofmann, S. Linz, R. Weigel, G. Fischer, and D. Kissinger, "A multiband 2-port VNA for biomedical applications based on two six-port-junctions," in *IEEE MTT-S Int. Microw. Symp. Dig.*, Seattle, WA, USA, Jun. 2013, pp. 1–3.

[53] B. Laemmle, K. Schmalz, C. Scheytt, D. Kissinger, and R. Weigel, "A 122 GHz multiprobe reflectometer for dielectric sensor readout in SiGe BiCMOS technology," in *Proc. IEEE Compound Semiconductor Integr. Circuit Symp. (CSICS)*, Waikoloa, HI, USA, Oct. 2011, pp. 1–4.

[54] S. Ulker and R. M. Weikle, "A millimeter-wave six-port reflectometer based on the sampled-transmission line architecture," *IEEE Microw. Wireless Compon. Lett.*, vol. 11, no. 8, pp. 340–342, Aug. 2001.

[55] J. Nehring, M. Bartels, R. Weigel, and D. Kissinger, "A permittivity sensitive PLL based on a silicon-integrated capacitive sensor for microwave biosensing applications," in *Proc. IEEE Topical Conf. Biomed. Wireless Technol., Netw., Sens. Syst. (BioWireleSS)*, San Diego, CA, USA, Jan. 2015, pp. 51–53.

[56] F. I. Jamal, S. Guha, M. H. Eissa, J. Wessel, and D. Kissinger, "A fully integrated low-power 30 GHz complex dielectric sensor in a 0.25-μm BiCMOS technology," *IEEE J. Electromagn., RF Microw. Med. Biol.*, vol. 2, no. 3, pp. 163–171, Sep. 2018.

[57] F. I. Jamal *et al.*, "Low-power miniature K-band sensors for dielectric characterization of biomaterials," *IEEE Trans. Microw. Theory Tech.*, vol. 65, no. 3, pp. 1012–1023, Mar. 2017.

[58] H. Wang, C.-C. Weng, and A. Hajimiri, "Phase noise and fundamental sensitivity of oscillator-based reactance sensors," *IEEE Trans. Microw. Theory Techn.*, vol. 61, no. 5, pp. 2215–2229, May 2013.

[59] C. Sideris, P. P. Khial, and A. Hajimiri, "Design and implementation of reference-free drift-cancelling CMOS magnetic sensors for biosensing applications," *IEEE J. Solid-State Circuits*, vol. 53, no. 11, pp. 3065–3075, Nov. 2018.

[60] T. Mitsunaka *et al.*, "CMOS biosensor IC focusing on dielectric relaxations of biological water with 120 and 60 GHz oscillator arrays," *IEEE J. Solid-State Circuits*, vol. 51, no. 11, pp. 2534–2544, Nov. 2016.

[61] V. Sekar, W. J. Torke, S. Palermo, and K. Entesari, "A selfsustained microwave system for dielectric-constant measurement of lossy organic liquids," *IEEE Trans. Microw. Theory Techn.*, vol. 60, no. 5, pp. 1444–1455, May 2012.

[62] O. Elhadidy, S. Shakib, K. Krenek, S. Palermo, and K. Entesari, "A wide-band fully-integrated CMOS ring-oscillator PLL-based complex dielectric spectroscopy system," *IEEE Trans. Circuits Syst. I, Reg. Papers*, vol. 62, no. 8, pp. 1940–1949, Aug. 2015.

[63] M. Babay *et al.*, "Highly sensitive capacitive sensor based on injection locked oscillators with ppm sensing resolution," in *IEEE MTT-S Int. Microw. Symp. Dig.*, Los Angeles, CA, USA, Aug. 2020, pp. 456–459.

[64] J. C. Chien and A. M. Niknejad, "Oscillator-based reactance sensors with injection locking for high-throughput flow cytometry using microwave dielectric spectroscopy," *IEEE J. Solid-State Circuits*, vol. 51, no. 2, pp. 457–472, Feb. 2016.

[65] P. Soltani Zarrin, F. Jamal, S. Guha, J. Wessel, D. Kissinger, and C. Wenger, "Design and fabrication of a BiCMOS dielectric sensor for viscosity measurements: A possible solution for early detection of COPD," *Biosensors*, vol. 8, no. 3, p. 78, Aug. 2018.

[66] J. Wessel, K. Schmalz, J. C. Scheytt, and D. Kissinger, "A 120-GHz electrical interferometer for contactless permittivity measurements with direct digital read-out," *IEEE Microw. Wireless Compon. Lett.*, vol. 27, no. 2, pp. 198–200, Feb. 2017.

[67] B. Laemmle, K. Schmalz, C. Scheytt, D. Kissinger, and R. Weigel, "A 62 GHz reflectometer for biomedical sensor readout in SiGe BiCMOS technology," in *Proc. IEEE 12th Topical Meeting Silicon Monolithic Integr. Circuits RF Syst.*, Santa Clara, CA, USA, Jan. 2012, pp. 45–48.

[68] B. Laemmle, K. Schmalz, J. C. Scheytt, R. Weigel, and D. Kissinger, "A 125-GHz permittivity sensor with read-out circuit in a 250-nm SiGe BiCMOS technology," *IEEE Trans. Microw. Theory Techn.*, vol. 61, no. 5, pp. 2185–2194, May 2013.

[69] Y. Cui and P. Wang, "The design and operation of ultra-sensitive and tunable radio-frequency interferometers," *IEEE Trans. Microw. Theory Techn.*, vol. 62, no. 12, pp. 3172–3182, Dec. 2014.

[70] F. A. Mubarak, R. Romano, L. Galatro, V. Mascolo, G. Rietveld, and M. Spirito, "Noise behavior and implementation of interferometerbased broadband VNA," *IEEE Trans. Microw. Theory Techn.*, vol. 67, no. 1, pp. 249–260, Jan. 2019.

[71] J. Wessel, K. Schmalz, J. C. Scheytt, and D. Kissinger, "Sensitive permittivity detector for dielectric samples at 120 GHz," in *Proc. IEEE Radio Wireless Symp. (RWS)*, Anaheim, CA, USA, Jan. 2018, pp. 136–138.

[72] B. Laemmle *et al.*, "A fully integrated 120-GHz six-port receiver frontend in a 130-nm SiGe BiCMOS technology," in *Proc. IEEE 13th Topics Meeting Silicon Monolithic Integr. Circuits RF Syst.*, Austin, TX, USA, Jan. 2013, pp. 129–131.

[73] M. Voelkel, M. Dietz, R. Weigel, A. Hagelauer, and D. Kissinger, "A low-power 60-GHz integrated sixport receiver front-end in a 130-nm BiCMOS technology," in *Proc. 12th Eur. Microw. Integr. Circuits Conf. (EuMIC)*, Nuremberg, Germany, Oct. 2017, pp. 73–76.

[74] M. Voelkel, H. Hirsch, M. Dietz, R. Weigel, A. Hagelauer, and D. Kissinger, "A low-power 120-GHz integrated sixport receiver frontend with digital adjustable gain in a 130-nm BiCMOS technology," in *Proc. IEEE Bipolar/BiCMOS Circuits Technol. Meeting (BCTM)*, Miami, FL, USA, Oct. 2017, pp. 82–85.

[75] C. Schmidt, J. Nehring, M. Dietz, R. Weigel, D. Kissinger, and A. Hagelauer, "A 10 Gb/s highly-integrated adaptive pseudo-noise transmitter for biomedical applications," in *Proc. IEEE Radio Wireless Symp. (RWS)*, Phoenix, AZ, USA, Jan. 2017, pp. 101–103.

[76] P. Rito, I. G. Lopez, M. Ko, A. C. Ulusoy, and D. Kissinger, "A 0.87-pJ/b 115-Gb/s 2^7-1 PRBS generator in 130-nm SiGe:C BiCMOS technology," *IEEE Solid-State Circuits Lett.*, vol. 1, no. 2, pp. 42–45, Feb. 2018.

[77] A. Gharib, R. Weigel, and D. Kissinger, "A versatile 10–80-Gb/s PRBS-based broadband transmitter with arbitrary 20–60-GHz spectrum shifting," *IEEE Trans. Microw. Theory Techn.*, vol. 64, no. 11, pp. 3654–3666, Nov. 2016.

[78] I. Nasr, M. Dudek, R. Weigel, and D. Kissinger, "A 33% tuning range high output power V-band superharmonic coupled quadrature VCO in SiGe technology," in *Proc. IEEE Radio Freq. Integr. Circuits Symp.*, Montreal, QC, Canada, Jun. 2012, pp. 301–304.

[79] G. Guariti, M. Hofmann, R. Weigel, G. Fischer, and D. Kissinger, "Determination of sugar concentration in aqueous solutions using ultrawideband microwave impedance spectroscopy," in *IEEE MTT-S Int. Microw. Symp. Dig.*, Seattle, WA, USA, Jun. 2013, pp. 1–3.

[80] C. Schmidt, M. Luebke, M. Dietz, R. Weigel, D. Kissinger, and A. Hagelauer, "Determination of changes in NaCl concentration in aqueous solutions using an M-sequence based sensor system," in *IEEE MTT-S Int. Microw. Symp. Dig.*, Gothenburg, Sweden, May 2017, pp. 1–4.

[81] M. Hamouda *et al.*, "A clock synchronization for M-sequence-based ultra-wideband systems," *IEEE Trans. Microw. Theory Techn.*, vol. 62, no. 12, pp. 3549–3561, Dec. 2014.

[82] M. Kmec, M. Helbig, J. Sachs, and P. Rauschenbach, "Integrated ultrawideband hardware for MIMO sensing using pn-sequence approach," in *Proc. IEEE Int. Conf. Ultra-Wideband*, Syracuse, NY, USA, Sep. 2012, pp. 333–337.

[83] A. Gharib, R. Weigel, and D. Kissinger, "Broadband circuit techniques for multi-terahertz gain-bandwidth-product low-power applications," *IEEE Trans. Microw. Theory Techn.*, vol. 63, no. 11, pp. 3701–3712, Nov. 2015.

[84] J. Nehring *et al.*, "Highly integrated 4–32-GHz two-port vector network analyzers for instrumentation and biomedical applications," *IEEE Trans. Microw. Theory Techn.*, vol. 65, no. 1, pp. 229–244, Jan. 2017.

[85] I. Nasr, J. Nehring, K. Aufinger, G. Fischer, R. Weigel, and D. Kissinger, "Single and dual-port 50–100-GHz highly integrated vector network analyzers with on-chip dielectric sensors," *IEEE Trans. Microw. Theory Techn.*, vol. 62, no. 9, pp. 2168–2179, Sep. 2014.

[86] J.-C. Chien, M. Anwar, E.-C. Yeh, L. P. Lee, and A. M. Niknejad, "A 1–50 GHz dielectric spectroscopy biosensor with integrated receiver front-end in 65 nm CMOS," in *IEEE MTT-S Int. Microw. Symp. Dig.*, Seattle, WA, USA, Jun. 2013, pp. 1–4.

[87] M. Bakhshiani, M. A. Suster, and P. Mohseni, "A broadband sensor interface IC for miniaturized dielectric spectroscopy from MHz to GHz," *IEEE J. Solid-State Circuits*, vol. 49, no. 8, pp. 1669–1681, Aug. 2014.

[88] M. M. Bajestan, A. A. Helmy, H. Hedayati, and K. Entesari, "A 0.62–10 GHz complex dielectric spectroscopy system in CMOS," *IEEE Trans. Microw. Theory Techn.*, vol. 62, no. 12, pp. 3522–3537, Dec. 2014.

[89] P. H. Siegel, A. Tang, G. Virbila, Y. Kim, M. C. F. Chang, and V. Pikov, "Compact non-invasive millimeter-wave glucose sensor," in *Proc. 40th Int. Conf. Infr., Millim., THz waves (IRMMW-THz)*, Hong Kong, Aug. 2015, pp. 1–3.

[90] X. Yang and A. Babakhani, "A full-duplex single-chip transceiver with self-interference cancellation in 0.13 μm SiGe BiCMOS for electron paramagnetic resonance spectroscopy," *IEEE J. Solid-State Circuits*, vol. 51, no. 10, pp. 2408–2419, Oct. 2016.

[91] H. Chung, Q. Ma, M. Sayginer, and G. M. Rebeiz, "A Packaged 0.01–26-GHz single-chip SiGe reflectometer for two-port vector network analyzers," *IEEE Trans. Microw. Theory Techn.*, vol. 68, no. 5, pp. 1794–1808, May 2020.

[92] J. Nehring, M. Dietz, K. Aufinger, G. Fischer, R. Weigel, and D. Kissinger, "A 4–32-GHz chipset for a highly integrated heterodyne two-port vector network analyzer," *IEEE Trans. Microw. Theory Techn.*, vol. 64, no. 3, pp. 892–905, Mar. 2016.

[93] I. Nasr, H. Knapp, K. Aufinger, R. Weigel, and D. Kissinger, "A 50–100-GHz highly integrated octave-bandwidth transmitter and receiver chipset in 0.35-μ m SiGe technology," *IEEE Trans. Microw. Theory Tech.*, vol. 62, no. 9, pp. 2118–2131, Sep. 2014.

[94] D. Wang, M. H. Eissa, K. Schmalz, T. Kampfe, and D. Kissinger, "240-GHz reflectometer-based dielectric sensor with integrated transducers in a 130-nm SiGe BiCMOS technology," *IEEE Trans. Microw. Theory Techn.*, vol. 69, no. 1, pp. 1027–1035, Jan. 2021.

[95] D. Wang *et al.*, "240-GHz four-channel power-tuning heterodyne sensing readout system with reflection and transmission measurements in a 130-nm SiGe BiCMOS technology," *IEEE Trans. Microw. Theory Techn.*, vol. 67, no. 12, pp. 5296–5306, Dec. 2019.

[96] T. W. Crowe, W. L. Bishop, D. W. Porterfield, J. L. Hesler, and R. M. Weikle, "Opening the terahertz window with integrated diode circuits," *IEEE J. Solid-State Circuits*, vol. 40, no. 10, pp. 2104–2110, Oct. 2005.

[97] G. Chattopadhyay, "Technology, capabilities, and performance of low power terahertz sources," *IEEE Trans. THz Sci. Technol.*, vol. 1, no. 1, pp. 33–53, Sep. 2011.

[98] I. Mehdi, J. V. Siles, C. Lee, and E. Schlecht, "THz diode technology: Status, prospects, and applications," *Proc. IEEE*, vol. 105, no. 6, pp. 990–1007, Jun. 2017.

[99] J. V. Siles, K. B. Cooper, C. Lee, R. H. Lin, G. Chattopadhyay, and I. Mehdi, "A new generation of room-temperature frequency-multiplied sources with up to $10\times$ higher output power in the 160-GHz–1.6-THz range," *IEEE Trans. THz Sci. Technol.*, vol. 8, no. 6, pp. 596–604, Nov. 2018.

[100] N. S. Barker, M. Bauwens, A. Lichtenberger, and R. Weikle, "Silicon-on-insulator substrates as a micromachining platform for advanced terahertz circuits," *Proc. IEEE*, vol. 105, no. 6, pp. 1105–1120, Jun. 2017.

[101] M. J. W. Rodwell *et al.*, "Active and nonlinear wave propagation devices in ultrafast electronics and optoelectronics," *Proc. IEEE*, vol. 82, no. 7, pp. 1037–1059, Jul. 1994.

[102] R. Y. Yu, M. Reddy, J. Pusl, S. T. Allen, M. Case, and M. J. W. Rodwell, "Millimeter-wave on-wafer waveform and network measurements using active probes," *IEEE Trans. Microw. Theory Techn.*, vol. 43, no. 4, pp. 721–729, Apr. 1995.

[103] O. Wohlgemuth, M. Rodwell, R. Reuter, J. Braunstein, and M. Schlechtweg, "Active probes for network analysis within 70–230 GHz," *IEEE Trans. Microw. Theory Tech.*, vol. 47, no. 12, pp. 2591–2598, Dec. 1999.

[104] M. J. W. Rodwell, M. Kamegawa, R. Yu, M. Case, E. Carman, and K. S. Giboney, "GaAs nonlinear transmission lines for picosecond pulse generation and millimeter-wave sampling," *IEEE Trans. Microw. Theory Techn.*, vol. 39, no. 7, pp. 1194–1204, Jul. 1991.

[105] G. M. Rebeiz, "Millimeter-wave and terahertz integrated circuit antennas," *Proc. IEEE*, vol. 80, no. 11, pp. 1748–1770, Nov. 1992.

[106] B. K. Kormanyos, P. H. Ostdiek, W. L. Bishop, T. W. Crowe, and G. M. Rebeiz, "A planar wideband 80–200 GHz subharmonic receiver," *IEEE Trans. Microw. Theory Techn.*, vol. 41, no. 10, pp. 1730–1737, Oct. 1993.

[107] S. Gearhart and G. Rebeiz, "A monolithic 250 GHz Schottky-diode receiver," *IEEE Trans. Microw. Theory Tech.*, vol. 42, no. 12, pp. 2504–2511, Dec. 1994.

[108] B.-H. Ku, H. Chung, and G. M. Rebeiz, "A 70–110 GHz single-chip SiGe reflectometer with integrated local oscillator quadrupler," in *IEEE MTT-S Int. Microw. Symp. Dig.*, Honolulu, HI, Jun. 2017, pp. 980–982.

[109] E. Turkmen and Y. Gurbuz, "A SiGe BiCMOS W-band single-chip frequency extension module for VNAs," *IEEE Trans. Microw. Theory Techn.*, vol. 68, no. 1, pp. 211–221, Jan. 2020.

[110] W. Aouimeur *et al.*, "A fully *in-situ* reflectometer in G band in 55 nm SiGe BiCMOS," in *Proc. Int. Workshop Integr. Non-linear Microw. Millimetre-wave Circuits (INMMIC)*, Jul. 2018, pp. 1–3.

[111] D. Wang *et al.*, "Integrated 240-GHz dielectric sensor with DC readout circuit in a 130-nm SiGe BiCMOS technology," *IEEE Trans. Microw. Theory Techn.*, vol. 66, no. 9, pp. 4232–4241, Sep. 2018.

[112] D. Wang, M. H. Eissa, K. Schmalz, T. Kampfe, and D. Kissinger, "480-GHz sensor with subharmonic mixer and integrated transducer in a 130-nm SiGe BiCMOS technology," *IEEE Microw. Wireless Compon. Lett.*, vol. 30, no. 9, pp. 908–911, Sep. 2020.

[113] C. Wang *et al.*, "Chip-scale molecular clock," *IEEE J. Solid-State Circuits*, vol. 54, no. 4, pp. 914–926, Apr. 2019.

[114] C. B. Kaynak *et al.*, "Modeling and characterization of BiCMOS embedded microfluidic platform for biosensing applications," in *Proc. IEEE Topical Conf. Biomed. Wireless Technol., Netw., Sens. Syst. (BioWireleSS)*, Newport Beach, CA, USA, Jan. 2014, pp. 46–48.

[115] M. Kaynak *et al.*, "BiCMOS integrated microfluidic platform for bio-MEMS applications," in *IEEE MTT-S Int. Microw. Symp. Dig.*, Tampa, FL, USA, Jun. 2014, pp. 1–3.

[116] K. Grenier *et al.*, "Integrated broadband microwave and microfluidic sensor dedicated to bioengineering," *IEEE Trans. Microw. Theory Techn.*, vol. 57, no. 12, pp. 3246–3253, Dec. 2009.

[117] J. C. Booth, N. D. Orloff, J. Mateu, M. Janezic, M. Rinehart, and J. A. Beall, "Quantitative permittivity measurements of nanoliter liquid volumes in microfluidic channels to 40 GHz," *IEEE Trans. Instrum. Meas.*, vol. 59, no. 12, pp. 3279–3288, Dec. 2010.

[118] S. Liu, I. Ocket, M. Cauwe, D. Schreurs, and B. Nauwelaers, "Sensitivity analysis of broadband on-wafer dielectric spectroscopy of yeast cell suspensions up to 110 GHz," *IEEE Microw. Wireless Compon. Lett.*, vol. 25, no. 3, pp. 199–201, Mar. 2015.

[119] L. Y. Zhang *et al.*, "Microwave biosensors for identifying cancer cell aggressiveness grade," in *IEEE MTT-S Int. Microw. Symp. Dig.*, Montreal, QC, Canada, Jun. 2012, pp. 1–3.

[120] J. Leroy *et al.*, "High frequency microfluidic biosensors for intracellular dielectric spectroscopy," in *IEEE MTT-S Int. Microw. Symp. Dig.*, Phoenix, AZ, USA, May 2015, pp. 1–4.

[121] J. Wesse, K. Schmalz, F. I. Jamal, and D. Kissinger, "Contactless investigation of dielectric samples with a high-Q millimeter-wave sensor," in *Proc. 40th Annu. Int. Conf. IEEE Eng. Med. Biol. Soc. (EMBC)*, Honolulu, HI, USA, Jul. 2018, pp. 1–4.

[122] K. Schmalz *et al.*, "A 120 GHz dielectric sensor in SiGe BiCMOS," *IEEE Microw. Wireless Compon. Lett.*, vol. 23, no. 1, pp. 46–48, Jan. 2013.

[123] C. Palego *et al.*, "BiCMOS microfluidic sensor for single cell label-free monitoring through microwave intermodulation," in *IEEE MTT-S Int. Microw. Symp. Dig.*, San Francisco, CA, USA, May 2016, pp. 1–4.

[124] K. Schmalz, N. Rothbart, P. F.-X. Neumaier, J. Borngraber, H.-W. Hubers, and D. Kissinger, "Gas spectroscopy system for breath analysis at mm-wave/THz using SiGe BiCMOS circuits," *IEEE Trans. Microw. Theory Techn.*, vol. 65, no. 5, pp. 1807–1818, May 2017.

[125] Y. Konishi, M. Kamegawa, M. Case, R. Yu, S. T. Allen, and M. J. W. Rodwell, "A broadband free-space millimeter-wave vector transmission measurement system," *IEEE Trans. Microw. Theory Techn.*, vol. 42, no. 7, pp. 1131–1139, Jul. 1994.

[126] A. Grichener and G. M. Rebeiz, "A 15–50-GHz quasi-optical scalar network analyzer scalable to terahertz frequencies," *IEEE Trans. Microw. Theory Techn.*, vol. 60, no. 8, pp. 2622–2633, Aug. 2012.

[127] A. J. Alazemi and G. M. Rebeiz, "A 100–300-GHz free-space scalar network analyzer using compact Tx and Rx modules," *IEEE Trans. Microw. Theory Techn.*, vol. 64, no. 11, pp. 4021–4029, Nov. 2016.

[128] N. Rothbart, K. Schmalz, J. Borngraber, D. Kissinger, and H.-W. Hubers, "Detection of volatile organic compounds in exhaled human breath by millimeter-wave/terahertz spectroscopy," in *Proc. 43rd Int. Conf. Infr., Millim., THz Waves (IRMMW-THz)*, Nagoya, Japan, Sep. 2018, pp. 1–2.

[129] J. Zhang, N. Sharma, W. Choi, D. Shim, Q. Zhong, and K. O. Kenneth, "85-to-127 GHz CMOS signal generation using a quadrature VCO with passive coupling and broadband harmonic combining for rotational spectroscopy," *IEEE J. Solid-State Circuits*, vol. 50, no. 6, pp. 1361–1371, Jun. 2015.

[130] D. J. Nemchick, B. J. Drouin, A. J. Tang, Y. Kim, and M.-C.-F. Chang, "Sub-Doppler spectroscopy with a CMOS transmitter," *IEEE Trans. THz Sci. Technol.*, vol. 8, no. 1, pp. 121–126, Jan. 2018.

[131] D. Nemchick et al., "180-GHz pulsed CMOS transmitter for molecular sensing," *IEEE Trans. THz Sci. Technol.*, vol. 11, no. 5, pp. 469–476, Sep. 2021.

[132] C. Wang and R. Han, "Dual-terahertz-comb spectrometer on CMOS for rapid, wide-range gas detection with absolute specificity," *IEEE J. Solid-State Circuits*, vol. 52, no. 12, pp. 3361–3372, Dec. 2017.

[133] K. Schmalz et al., "245-GHz transmitter array in SiGe BiCMOS for gas spectroscopy," *IEEE Trans. THz Sci. Technol.*, vol. 6, no. 2, pp. 318–327, Mar. 2016.

[134] K. Schmalz, N. Rothbart, M. H. Eissa, J. Borngräber, D. Kissinger, and H.-W. Hübers, "Transmitters and receivers in SiGe BiCMOS technology for sensitive gas spectroscopy at 222–270 GHz," *AIP Advances*, vol. 9, no. 1, p. 15213, Jan. 2019.

[135] K. Schmalz et al., "Tunable 500 GHz sensor system in SiGe technology for gas spectroscopy," *Electron. Lett.*, vol. 51, no. 17, pp. 1345–1347, Aug. 2015.

[136] A. Güner, T. Mausolf, J. Wessel, D. Kissinger, and K. Schmalz, "A 440–540 GHz sub-harmonic mixer in 130 nm SiGe BiCMOS," *IEEE Microw. Wireless Compon. Lett.*, vol. 30, no. 12, pp. 1161–1164, Dec. 2020.

[137] A. Güner, T. Mausolf, J. Wessel, D. Kissinger, and K. Schmalz, "A 440–540 GHz transmitter in 130 nm SiGe BiCMOS technology," *IEEE Microw. Wireless Compon. Lett.*, vol. 31, no. 6, pp. 779–782, Jun. 2021.

[138] N. Rothbart, K. Schmalz, J. Borngraber, D. Kissinger, and H.-W. Hubers, "Gas spectroscopy by voltage-frequency tuning of a 245 GHz SiGe transmitter and receiver," *IEEE Sensors J.*, vol. 16, no. 24, pp. 8863–8864, Dec. 2016.

[139] D. Wagner et al., "Application of microwave sensor technology in cardiovascular disease for plaque detection," *Current Directions Biomed. Eng.*, vol. 2, no. 1, pp. 273–277, Oct. 2016.

[140] V. Lammert et al., "A K-band complex permittivity sensor for biomedical applications in 130-nm SiGe BiCMOS," *IEEE Trans. Circuits Syst. II, Exp. Briefs*, vol. 66, no. 10, pp. 1628–1632, Oct. 2019.

[141] D. Wagner et al., "Packaging of a BiCMOS sensor on a catheter tip for the characterization of atherosclerotic plaque," in *Proc. IEEE Electron. Syst. Integr. Technol. Conf.*, Grenoble, France, Sep. 2016, pp. 1–3.

[142] C. Baer et al., "A millimeter-wave based measuring method for the differentiation of atherosclerotic plaques," in *IEEE MTT-S Int. Microw. Symp. Dig.*, Singapore, Dec. 2013, pp. 1–4.

[143] V. Issakov et al., "Fully autonomous system-on-board with complex permittivity sensors and 60 GHz transmitter for biomedical implant applications," in *Proc. IEEE Radio Freq. Integr. Circuits Symp. (RFIC)*, Aug. 2020, pp. 159–162.

[144] M. Inac et al., "BiCMOS integrated microfluidic packaging by wafer bonding for lab-on-chip applications," in *Proc. IEEE 67th Electron. Compon. Technol. Conf. (ECTC)*, Orlando, FL, USA, May 2017, pp. 786–791.

[145] W. Su, B. S. Cook, and M. M. Tentzeris, "Additively manufactured microfluidics-based 'peel-and-replace' RF sensors for wearable applications," *IEEE Trans. Microw. Theory Tech.*, vol. 64, no. 6, pp. 1928–1936, Jun. 2016.

[146] M. Mueh, M. Maasch, R. A. Knieß, H. U. Göringer, and C. Damm, "Detection of African trypanosomes using asymmetric double-split ring based THz sensors," *IEEE J. Electromagn., RF Microw. Med. Biol.*, vol. 1, no. 2, pp. 66–73, Dec. 2017.

[147] P. Steglich, S. Bondarenko, C. Mai, M. Paul, M. G. Weller, and A. Mai, "CMOS-compatible silicon photonic sensor for refractive index sensing using local back-side release," *IEEE Photon. Technol. Lett.*, vol. 32, no. 19, pp. 1241–1244, Oct. 1, 2020.

[148] C. Mai, P. Steglich, M. Fraschke, and A. Mai, "Back-side release of slot waveguides for the integration of functional materials in a silicon photonic technology with a full BEOL," *IEEE Trans. Compon., Package., Manuf. Technol.*, vol. 10, no. 9, pp. 1569–1574, Sep. 2020.

[149] P. Steglich et al., "Hybrid-waveguide ring resonator for biochemical sensing," *IEEE Sensors J.*, vol. 17, no. 15, pp. 4781–4790, Aug. 2017.

[150] D. Knoll et al., "BiCMOS silicon photonics platform for fabrication of high-bandwidth electronic-photonic integrated circuits," in *Proc. IEEE 16th Top. Meeting Silicon Monolithic Integr. Circuits RF Syst.*, Austin, TX, USA, Jan. 2016, pp. 46–49.

[151] L. Zhang and A. M. Niknejad, "Design and analysis of a microwave-optical dual modality biomolecular sensing platform," *IEEE J. Solid-State Circuits*, vol. 55, no. 3, pp. 639–649, Mar. 2020.

Dietmar Kissinger (Senior Member, IEEE) received the Dipl.-Ing., Dr.-Ing., and habil. degrees from Friedrich-Alexander-Universität Erlangen-Nürnberg, Erlangen, Germany, in 2007, 2011, and 2014, respectively, all in electrical engineering.

From 2007 to 2010, he was with the Automotive Radar Group, Danube Integrated Circuit Engineering, Linz, Austria, where he was a System and Application Engineer. From 2010 to 2014, he was a Lecturer and the Head of the Radio Frequency Integrated Sensors Group, Institute for Electronics Engineering, Erlangen. From 2015 to 2018, he was with Technische Universität Berlin, Berlin, Germany, and the Head of the Circuit Design Department, Leibniz-Institut für innovative Mikroelektronik (IHP), Frankfurt (Oder), Germany. Since 2019, he has been a Full Professor of high-frequency circuit design with Ulm University, Ulm, Germany, and the Head of the Institute of Electronic Devices and Circuits, Ulm. He has authored or coauthored over 350 technical papers and holds more than ten patents. His current research interests include silicon high-frequency and high-speed integrated circuits and systems for communication and automotive, industrial, security, and biomedical sensing applications.

Dr. Kissinger was a member of the 2013 and 2017 European Microwave Week (EuMW) Organizing Committee and the 2018 IEEE Microwave Theory and Technology Society (MTT-S) International Microwave Symposium (IMS) Steering Committee. He is a member of the European Microwave Association (EuMA), the German Association of Electrical Engineers [Verein Deutscher Elektrotechniker (VDE)], and the Technical Program Committee (TPC) of the European Solid-State Circuits Conference (ESSCIRC). He is an elected member of the IEEE MTT-S Administrative Committee. He received the 2017 IEEE MTT-S Outstanding Young Engineer Award, the 2017 VDE/Verein Deutscher Ingenieure (VDI) Gesellschaft Mikroelektronik, Mikrosystem-und Feinwerktechnik (GMM) Prize, and the 2018 VDE Informationstechnische Gesellschaft (ITG) Prize. He was a co-recipient of over ten best paper awards. He was a two-time Chair of the IEEE Topical Conference on Wireless Sensors and Sensor Networks (WiSNet) and the IEEE Topical Conference on Biomedical Wireless Technologies, Networks and Sensing Systems (BioWireless). He served as the Executive Committee Chair of the Radio and Wireless Week (RWW). He serves as the Chair of the IEEE MTT-S Technical Coordination and Future Directions Committee and the TPC Chair of the 2022 German Microwave Conference (GeMiC). He was the Chair of the IEEE MTT-S Technical Committee on Microwave and Millimeter-Wave Integrated Circuits (MTT-14). He was a nine-time Guest Editor of *IEEE Microwave Magazine* and served as an Associate Editor for the IEEE TRANSACTIONS ON MICROWAVE THEORY AND TECHNIQUES.

Mehmet Kaynak (Member, IEEE) received the B.S. degree from the Electronics and Communication Engineering Department, Istanbul Technical University (ITU), Istanbul, Turkey, in 2004, the M.S. degree from the Microelectronic Program, Sabanci University, Istanbul, in 2006, and the Ph.D. degree from the Technical University of Berlin, Berlin, Germany, in 2014.

He joined the Technology Group, Leibniz-Institut für innovative Mikroelektronik (IHP), Frankfurt (Oder), Germany, in 2008. From 2008 to 2015, he has led the MEMS development at IHP. From 2015 to 2020, he was the Head of the Department of Technology, IHP.

Andreas Mai (Member, IEEE) received the Diploma degree in physics and the Dr. rer. nat. and Dr.-Ing. habil. degrees from the Brandenburg University of Technology Cottbus-Senftenberg, Cottbus, Germany, in 2006, 2010, and 2022, respectively.

He joined the Department of Technology, Leibniz-Institut für innovative Mikroelektronik (IHP), Frankfurt (Oder), Germany in 2006, where he was a Group Leader of the Process Integration Team with the responsibility for service, research activities, and technology developments. Since 2015, he has been a Department Head of Technology for Smart Systems, IHP, with responsibilities for the 8-in. pilot line operation and management of research and service activities. He is currently a Professor of micro- and nanoelectronics with the Technical University of Applied Sciences Wildau, Wildau, Germany, where he leads the JointLab and Institute of Applied Physics. His research interests include the development of functional diversification of 130-nm SiGe BiCMOS and photonic technologies for millimeter-wave and sensor applications.

Dr. Mai is the Chair of the Electrochemical Society (ECS) SiGe Process and Integration Committee.